An Extracellular Cu^{2+} Binding Site in the Voltage Sensor of BK and Shaker Potassium Channels

Zhongming Ma, Kin Yu Wong, and Frank T. Horrigan

Department of Physiology, University of Pennsylvania School of Medicine, Philadelphia, PA 19104

Copper is an essential trace element that may serve as a signaling molecule in the nervous system. Here we show that extracellular Cu^{2+} is a potent inhibitor of BK and Shaker K^+ channels. At low micromolar concentrations, Cu^{2+} rapidly and reversibly reduces macrosocopic K^+ conductance (G_K) evoked from mSlo1 BK channels by membrane depolarization. G_K is reduced in a dose-dependent manner with an IC_{50} and Hill coefficient of ~2 μM and 1.0, respectively. Saturating 100 μM Cu^{2+} shifts the G_K-V relation by +74 mV and reduces G_{Kmax} by 27% without affecting single channel conductance. However, 100 μM Cu^{2+} fails to inhibit G_K when applied during membrane depolarization, suggesting that Cu^{2+} interacts poorly with the activated channel. Of other transition metal ions tested, only Zn^{2+} and Cd^{2+} had significant effects at 100 μM with IC_{50}s > 0.5 mM, suggesting the binding site is Cu^{2+} selective. Mutation of external Cys or His residues did not alter Cu^{2+} sensitivity. However, four putative Cu^{2+}-coordinating residues were identified (D133, Q151, D153, and R207) in transmembrane segments S1, S2, and S4 of the mSlo1 voltage sensor, based on the ability of substitutions at these positions to alter Cu^{2+} and/or Cd^{2+} sensitivity. Consistent with the presence of acidic residues in the binding site, Cu^{2+} sensitivity was reduced at low extracellular pH. The three charged positions in S1, S2, and S4 are highly conserved among voltage-gated channels and could play a general role in metal sensitivity. We demonstrate that Shaker, like mSlo1, is much more sensitive to Cu^{2+} than Zn^{2+} and that sensitivity to these metals is altered by mutating the conserved positions in S1 or S4 or reducing pH. Our results suggest that the voltage sensor forms a state- and pH-dependent, metal-selective binding pocket that may be occupied by Cu^{2+} at physiologically relevant concentrations to inhibit activation of BK and other channels.

The Journal of General Physiology

INTRODUCTION

Copper and zinc are essential components of many enzymes and other proteins and, aside from iron, are the most abundant trace elements in the human body. Both metals are present in plasma at ~15 μM and accumulate in the brain at concentrations on the order of 100 μM (Osterberg, 1980; Linder and Hazegh-Azam, 1996; Takeda, 2000; Mathie et al., 2006). While most of this metal is protein bound, Cu^{2+} and Zn^{2+} may function as signaling molecules that are concentrated in synaptic vesicles and coreleased with neurotransmitters (Frederickson et al., 2005). Nerve terminals in certain areas of the brain contain copper or zinc that is histochemically stainable and therefore present in a free or loosely bound form (Slomianka et al., 1990; Sato et al., 1994; Ono and Cherian, 1999; Takeda, 2000). Brain slice and synaptosome preparations release Cu^{2+} and Zn^{2+} in a Ca^{2+}-dependent manner upon membrane depolarization (Howell et al., 1984; Hartter and Barnea, 1988), suggesting that total concentrations in the synaptic cleft may approach 100–250 μM Cu^{2+} (Kardos et al., 1989) or 300 μM Zn^{2+} (Assaf and Chung, 1984). The fraction of this release that can interact with synaptic proteins has not been clearly established, but indicator dye measurements suggest free synaptic concentrations on the order of 3 μM Cu^{2+} (Hopt et al., 2003) or 10 μM Zn^{2+} (Li et al., 2001; Thompson et al., 2002; Frederickson et al., 2006) are possible. Consequently there is considerable interest in understanding how low μM concentrations of Cu^{2+} or Zn^{2+} may interact with synaptic proteins such as ion channels. Such interactions could potentially play a role in normal synaptic physiology as well as disease states with neurological symptoms including inherited disorders of Cu^{2+} transport (Wilsons's and Menke's disease) and neurodegenerative diseases such as Alzheimers, Parkinsons, Creutzfeldt-Jakob disease, and amyotrophic lateral sclerosis, which are associated with altered Cu^{2+} and/or Zn^{2+} homeostasis (Bush, 2000; Frederickson et al., 2005; Mathie et al., 2006). In a broader sense, the ability of ion channels to detect trace metal ions is also relevant to understanding transition metal toxicity (Kiss and Osipenko, 1994).

Extracellular metal ions are well known to influence ion channel function by altering gating or blocking the pore (Elinder and Arhem, 2003). A variety of channels are extremely sensitive to Cu^{2+} and/or Zn^{2+} at concentrations <10 μM including subtypes of glutamate, glycine, Gaba(A), P2X, and acetylcholine receptors (Mathie et al., 2006; Huidobro-Toro et al., 2008), two-pore-domain K^+ (K2P) channels (Gruss et al., 2004),

Correspondence to Frank T. Horrigan:
Horrigan@mail.med.upenn.edu

Abbreviation used in this paper: WT, wild type.

The Rockefeller University Press $30.00
J. Gen. Physiol. Vol. 131 No. 5 483–502
www.jgp.org/cgi/doi/10.1085/jgp.200809980

and voltage-gated K^+ (Kv1.3) (Teisseyre and Mozrzymas, 2006), Na^+ (Nav1.5) (Mathie et al., 2006), and Ca^{2+} channels including a number of high voltage–activated types (Castelli et al., 2003) and Cav3.2 (Jeong et al., 2003). While the number of voltage-dependent channels identified as extremely sensitive to Cu^{2+} or Zn^{2+} is small, many voltage-gated channels exhibit responses to higher concentrations of metals (e.g., ≥100 µM) that have been studied in detail and provide a mechanistic basis for understanding of metal action (Elinder and Arhem, 2003).

Many transition metals at millimolar concentrations can shift the voltage dependence of channel activation in a nonspecific manner by screening surface charge on the channel and lipid bilayer. Similarly, metal occupancy of specific sites on channels outside of the voltage sensor can influence gating through electrostatic interaction with the voltage sensor (Elinder and Arhem, 2003; Yang et al., 2007). Metals can also bind directly to the voltage sensor and have been proposed to inhibit voltage sensor activation in squid axon K^+ and Na^+ channels by stabilizing the resting conformation (Gilly and Armstrong, 1982a,b). Acidic residues in the S2 and S3 segments of the voltage sensor domain of dEAG and hERG channels have been identified as putative coordinating sites for a variety of divalent cations (Silverman et al., 2000; Silverman et al., 2004; Fernandez et al., 2005). A key histidine in the S3–S4 loop of the voltage-sensor is also critical for the extreme metal sensitivity of Cav3.2 (Kang et al., 2006; Nelson et al., 2007). Finally, extracellular metals can enhance inactivation (Yellen et al., 1994), and the ability of Zn^{2+} to reduce the maximal conductance (G_{KMAX}) of Kv1.5 channels has been attributed to such a mechanism, involving putative coordinating residues in the pore domain (Kehl et al., 2002).

Although various mechanisms and sites of metal action in voltage-gated channels have been described, many fundamental questions remain unanswered. Most of the above examples involve channels with relatively low (mM) affinity and selectivity for metals. Which of these mechanisms, if any, apply to channels that are sensitive to metals at concentrations on the order of 1 µM? To what extent can channels distinguish between closely related metal ions like Cu^{2+} and Zn^{2+}, and what mechanisms underlie selectivity? How are metals coordinated by voltage sensors, and how do such sites change with voltage sensor activation to interact with metals in a state-dependent manner?

Large conductance BK-type K channels (Slo1) are activated by voltage and intracellular Ca^{2+}, play an important role in synaptic physiology (Faber and Sah, 2003), and are present in parts of the brain (Misonou et al., 2006) that contain synaptic Cu^{2+} and Zn^{2+} (Kozma et al., 1981; Slomianka et al., 1990; Sato et al., 1994; Ono and Cherian, 1999; Takeda, 2000). A previous study reported that BK channels from rat skeletal muscle are insensitive to 1–10 µM Cu^{2+} or 100 µM Zn^{2+}, but their activity is reduced slowly and irreversibly by prolonged exposure to ≥20 µM Cu^{2+} (Morera et al., 2003). This inhibitory effect of Cu^{2+} occurred with a substantial 20-min delay at 20 µM, was partially reversed by the reducing agent dithiothreitol (DTT), was reduced by mutation of extracellular Cys residues, and was attributed to a pro-oxidant effect of copper on amino acid sulfhydryl groups. By contrast, we demonstrate here an acute inhibitory effect of extracellular Cu^{2+} on the activation of heterologously expressed mSlo1 BK channels, characterized by an IC_{50} of only 2 µM. The inhibition of G_K by Cu^{2+} is rapid, readily reversible, unaffected by removal of extracellular Cys residues, and therefore unlikely to involve channel oxidation. Instead, our results suggest that Cu^{2+} binds between transmembrane segments S1, S2, and S4 of the resting voltage sensor to inhibit voltage sensor activation. The binding site appears to be remarkably selective for Cu^{2+} over other transition metals (Zn^{2+}, Cd^{2+}, Mn^{2+}, Fe^{3+}, Co^{2+}, and Ni^{2+}). The state dependence and selectivity of Cu^{2+} action may explain why the extreme metal sensitivity of the BK channel has not been described previously. We also demonstrate a response of Shaker K^+ channels to micromolar Cu^{2+} involving some of the same voltage sensor positions that are important in mSlo1. The ability of K^+ channel voltage sensors to coordinate Cu^{2+} and Zn^{2+} has implications for understanding not only mechanisms of metal action in BK and related voltage-gated channels but also the conformational changes associated with voltage sensor activation.

MATERIALS AND METHODS

Channel Expression and Molecular Biology

BK channels experiments were performed with the mbr5 clone of the mouse homologue of the Slo1 gene (mSlo1) (Butler et al., 1993). The clone was propagated and cRNA transcribed as described previously (Cox et al., 1997). The wild-type (WT) Shaker channel was Shaker H4 with residues 6–46 deleted to remove N-type inactivation and T449V to inhibit C-type inactivation. *Xenopus* oocytes were injected with ~0.5–50 ng cRNA, incubated at 18°C, and studied 2–7 d after injection. Site-directed mutagenesis was performed with the QuikChange XL site-directed mutagenesis kit (Stratagene) and confirmed by sequencing.

Electrophysiology and Data Analysis

Currents were recorded using the patch clamp technique in the outside-out configuration (Hamill et al., 1981), at room temperature (20–22°C). For BK channels, the internal solution contained (in mM) 110 $KMeSO_3$, 20 HEPES, and 40 µM (+)-18-crown-6-tetracarboxylic acid (18C6TA) to chelate contaminant Ba^{2+} (Diaz et al., 1996; Neyton, 1996). In addition, "0 Ca^{2+}" solution contained 5 mM EGTA, reducing free Ca^{2+} to an estimated 0.8 nM, and Ca^{2+} solutions contained 5 mM HEDTA. [Ca^{2+}] reported as 1, 3, 5, and 10 µM correspond to concentrations of 0.87, 2.4, 3.98, and 8.7 µM measured with a Ca^{2+} electrode (Orion Research Inc.). Ca^{2+} was added as $CaCl_2$ and [Cl^-] was adjusted to 10 mM with HCl. The standard external solution contained 110 $KMeSO_3$, 2 $MgCl_2$, 6 HCl, 10 MES, 10 MOPS. MES and MOPS buffers were used rather than HEPES, which is known to chelate Cu^{2+} (Mash et al., 2003; Sokolowska and Bal, 2005). For Shaker channels, the

internal solution contained (in mM) 160 KCl, 11 EGTA, 20 HEPES, and the standard external solution contained 155 NaCl, 5 KCl, $3CaCl_2$, 1 $MgCl_2$, 10 MES, 10 MOPS. The pH of all solutions were adjusted to 7.2, except for pH experiments where the external pH was adjusted from 5.2 to 8.14. Solutions were exchanged by washing the chamber with 20 volumes of solution (~5 ml), with the exception of experiments in Fig. 1 B and Fig. 3 (C and D), which used a rapid perfusion system (SF-77B Perfusion Fast-Step, Warner).

Metal stock solutions of 0.1 M or 1 M nitrate salt were prepared in distilled water, stored at 4°C, and diluted to their final concentration in standard external solution immediately before use. Metals were not buffered and are described by their nominal concentrations. All chemicals were Ultra-grade from Sigma-Aldrich including MES and MOPS (>99.5%) and transition metal nitrate salts (>99.99%) to avoid metal contamination. Metals were washed out using a 5 mM EGTA solution prepared from the standard external solution with a total of 2.43 mM Mg^{2+} to maintain free Mg^{2+} at 2 mM. Following application of EGTA solution, the chamber was washed with standard external solution before recording currents. We did not observe any effect on mSlo1 or Shaker channel function of switching between standard extracellular solutions and EGTA solution, suggesting any metal contamination is below the channel's detection limit.

Free metal concentrations can be influenced by the formation of chloride complexes and the limited solubility of metal hydroxides at neutral pH. Chloride is primarily a concern for Cd^{2+}, estimated to reduce $[Cd^{2+}]_{free}$ to 49% of its nominal concentration in mSlo1 solution (10 Cl^-) based on equilibrium constants reported by Pivovarov (2005). By contrast, free Cu^{2+} and Zn^{2+} should only be reduced to 99% and 99.5% of their nominal concentration in mSlo1 solution or 86% and 90% in Shaker solution (160 Cl^-) (Pivovarov, 2005). The poor solubility of copper hydroxide ($Cu(OH)_2$) can limit $[Cu^{2+}]_{free}$ to equilibrium concentrations on the order of 100 µM, but hydroxide formation is slow and can require many hours to equilibrate (Hidmi and Edwards, 1999). Consequently, metal solutions were prepared and used within 30 min to minimize hydroxide formation, and discarded if any precipitate was observed. To evaluate the free copper concentration in our experimental solutions, $[Cu^{2+}]$ measured with a Cu^{2+} electrode (Orion Research Inc.) was compared in equivalent solutions at pH 7.2 and an acidic pH 5.8 where hydroxide formation is minimal. The results were indistinguishable after correcting for a constant shift in electrode potential due to pH, indicating that the concentrations used in experiments are very close to the nominal concentrations. In both cases, electrode potentials varied linearly with $\log[Cu^{2+}]$ over a range of 0.1 to 1000 µM with slopes (~30 mV/10-fold change) within the range specified by the manufacturer.

Data were acquired with an Axopatch 200B amplifier (Molecular Devices Corp.) in patch mode with Axopatch's filter set at 100 kHz. Currents were filtered by an 8-pole Bessel filter (Frequency Device, Inc.) at 20 kHz and sampled at 100 kHz with an 18-bit A/D converter (Instrutech ITC-18). A P/4 protocol was used for leak subtraction (Armstrong and Bezanilla, 1974) with a holding potential of −80 or −90 mV for mSlo1 or Shaker channels, respectively. Electrodes were made from thick-walled 1010 glass (World Precision Instruments, Inc.). The electrode's resistance in the bath solution (1.0–2.5 MΩ) was used as an estimate of series resistance (R_S) for correcting the voltage at which macroscopic I_K was recorded. Series resistance error was <15 mV for all data presented. A Macintosh-based computer system was used in combination with Pulse Control acquisition software (Herrington and Bookman, 1995) and Igor Pro for graphing and data analysis (WaveMetrics, Inc.). A Levenberg-Marquardt algorithm was used to perform nonlinear least-squared fits. Data are presented as mean ± SEM.

For mSlo1 channels, open probability (P_O) was estimated over a wide voltage range by recording macroscopic I_K when NP_O was high (>5), and single channel currents in the same patch when NP_O was low (<10). Macroscopic conductance (G_K) was determined from tail currents at −80 mV following 30-ms voltage pulses (at 5-s intervals), and was normalized by G_{Kmax} in the absence of metals. At more negative voltages, NP_O was determined from steady-state recordings of 1–60-s duration that were digitally filtered at 5 kHz. NP_O was determined from all-points amplitude histograms by measuring the fraction of time spent (P_K) at each open level (k) using a half-amplitude criteria and summing their contributions $NP_o = \Sigma k P_k$. P_o was then determined by estimating N from G_{Kmax} ($N = G_{Kmax}/\gamma_K$, where γ_K is the single channel conductance at −80 mV).

G_K-V and dose–response relations were characterized by Boltzmann functions and Hill equations, respectively, as data descriptor functions. Boltzmann functions were of the form $G_K(V) = G_{Kmax}\,[1 + \exp(-z_{APP}(V - V_{0.5})/kT)]^{-1}$, where z_{APP} is the apparent charge movement. Hill equations were of the form $Y([L]) = Y_0 + (Y_{Max} - Y_0)*[L]^{nH}/([L]^{nH} + IC_{50}{}^{nH})$, where [L] is the ligand concentration, Y_0 and Y_{Max} are values of the dependent variable (Y) at zero and saturating [L], and n_H is the Hill coefficient.

RESULTS

Extracellular Cu^{2+} Inhibits BK Channel Activation

Macroscopic BK channel potassium current (I_K) evoked by membrane depolarization is reduced markedly and rapidly by 100 µM extracellular Cu^{2+} (Fig. 1, A and B). I_K was recorded in the absence of intracellular Ca^{2+} (0 Ca^{2+}) from outside-out patches expressing mSlo1 channels (Fig. 1 A). Steady-state inhibition of I_K was achieved within a fraction of a second of applying 100 µM Cu^{2+} to a patch (Fig. 1 B) and completely reversed by washing out Cu^{2+} with 5 mM EGTA (Fig. 1 A). Thus I_K inhibition does not reflect oxidation of BK channels by Cu^{2+}, which reportedly proceeds with a 1-min delay in 100 µM Cu^{2+} and is not reversed by removal of Cu^{2+} (Morera et al., 2003). We did not observe any irreversible effects even after more than 20 min in 100 µM Cu^{2+}.

Both outward current during a depolarization and inward tail current following the pulse were similarly reduced by 100 µM Cu^{2+} (Fig. 1 A), and the single channel current–voltage relation was unaffected (Fig. 1 C). Thus Cu^{2+} does not reduce I_K by acting like many intracellular divalent cations to rapidly block the BK channel pore and reduce single channel conductance in a voltage-dependent manner (Oberhauser et al., 1988; Ferguson, 1991). Instead, Cu^{2+} inhibits BK channel activation, shifting the half-activation voltage ($V_{0.5}$) of the G_K-V relation to more positive voltages by +82 mV and decreasing G_{Kmax} by ~18% in 1000 µM Cu^{2+} as estimated by fits to Boltzmann functions (Fig. 1 D). Increasing $[Cu^{2+}]$ from 100 to 1000 µM produced no additional reduction in G_K (Fig. 1 D), indicating that 100 µM is a saturating concentration and further supporting that Cu^{2+} does not act by occluding the pore. I_K kinetics were also altered by 100 µM Cu^{2+} in a manner consistent with a positive shift in the G_K-V relation, slowing the activation time constant 1.6-fold at +220 mV (Fig. 1 E) and speeding deactivation 1.4-fold at −80 mV (Fig. 1 F).

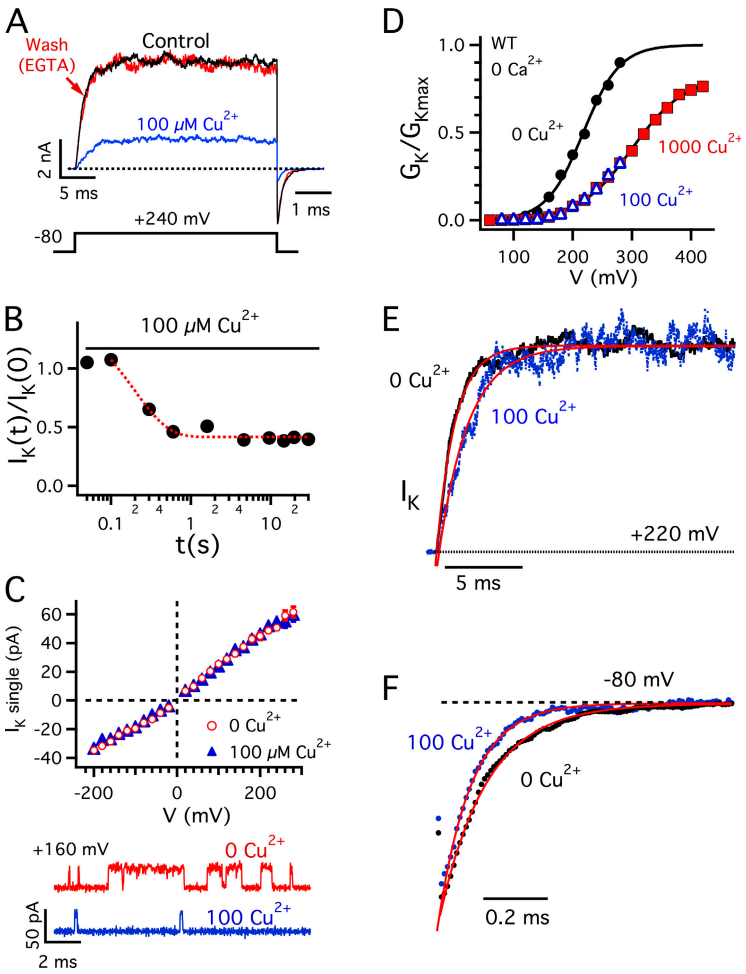

Figure 1. Extracellular Cu^{2+} inhibits mSlo1 activation. (A) I_k evoked in response to a pulse to +240 mV from a holding potential of −80 mV (0 Ca^{2+}). Currents in 0 Cu^{2+} (control), 100 μM Cu^{2+}, and washout with 5 mM EGTA were recorded from the same patch. Tail currents are shown on an expanded time scale, and have their own time scale bar. (B) The time course of inhibition by 100 μM Cu^{2+} was measured with a double pulse protocol. The ratio of steady-state I_K during two 30-ms test pulses to +220 mV is plotted against the interval between pulses (t). Cu^{2+} was applied at −80 mV with rapid perfusion immediately following the first test pulse ($t = 0$). I_K is inhibited rapidly ($\tau = 0.2$ s, dotted curve) following a delay of ~0.1 s likely representing the time for Cu^{2+} to reach the patch. (C) Single channel I_K-V relation is unaffected by 100 μM Cu^{2+} (top). Representative traces at +160 mV from a single channel patch show a marked decrease in P_O (bottom). (D) Normalized G_K-V relations determined in 0 Cu^{2+} (●), 100 μM Cu^{2+} (△), and 1000 μM Cu^{2+} (■) for the same patch are fit by Boltzmann functions (0 Ca: $G_{Kmax} = 1$, $V_{0.5} = 218$ mV, $Z_{app} = 0.82$ *e*; 1000 Cu^{2+}: $G_{Kmax} = 0.81$, $V_{0.5} = 300$ mV, $Z_{app} = 0.57$ *e*). (E) Normalized outward I_K at +220 mV and (F) tail currents at −80 mV in 0 Cu^{2+} and 100 μM Cu^{2+} are fit by exponential functions. 100 μM Cu^{2+} increased the activation time constant 1.6-fold from 1.25 to 1.98 ms and decreased the deactivation time constant 1.4-fold from 153 to 108 μs.

BK Channels Are Sensitive to Low Micromolar Cu^{2+}

The sensitivity of mSlo1 channels to Cu^{2+} is indicated by mean G_K-V relations measured in different [Cu^{2+}], from 0 to 200 μM (Fig. 2 A). Currents were recorded in the presence of 3 μM intracellular Ca^{2+} to shift activation to more negative voltages and facilitate measurements in the presence of Cu^{2+}. Similar to the results in 0 Ca^{2+}, 100 μM Cu^{2+} shifted the G_K-V by +74 ± 1 mV and reduced G_{Kmax} by 27 ± 1% (Fig. 2 A). Normalized G_K-Vs in Fig. 2 B better illustrate the changes in $V_{0.5}$. I_K kinetics in 3 μM Ca^{2+} were altered by 100 μM Cu^{2+} more than in 0 Ca^{2+} (slowed 3.3 ± 0.1-fold at +220 mV, speeded 2.5 ± 0.2-fold at −80 mV). However, activation remained fast compared with the 30-ms voltage pulse duration (e.g., $\tau(I_K) = 3.1 \pm 0.1$ ms at +220 mV), indicating that G_K-V relations in Fig. 2 A should accurately represent the steady-state gating of Cu^{2+}-bound channels.

Effects of Cu^{2+} on G_K were detectable at submicromolar concentrations and an approximate half-maximal response was observed in 2.5 μM Cu^{2+} (filled squares, Fig. 2, A and B). A dose–response relation determined by plotting the shift in half-activation voltage ($\Delta V_{0.5}$) versus [Cu^{2+}] (filled symbols, Fig. 2 C) is fit by a Hill equation (see Materials and methods) with an IC_{50} of 1.97 ± 0.25 μM and Hill coefficient (n_H) of 1.01 ± 0.09. Dose–response curves were also obtained by plotting G_K-[Cu^{2+}] relations at single voltages as illustrated in Fig. 2 C (open symbols) for 110, 150, and 190 mV. The IC_{50} and Hill coefficient obtained by fitting G_K-[Cu^{2+}] relations at different voltages are plotted in Fig. 2, D and E, respectively (filled symbols), and were similar to those derived from $\Delta V_{0.5}$ (Fig. 2, D and E, dotted lines) with IC_{50} values of 0.53–2.24 μM and n_H ranging from 0.9 to 1.2. Similar results were also obtained from G_K-[Cu^{2+}] relations in 0 Ca^{2+} (Fig. 2, D and E, open symbols). The voltage dependence of IC_{50} and n_H may reflect that the steepness of G_K-V curves was also reduced by Cu^{2+} as illustrated in Fig. 2 F by plotting the apparent charge from Boltzmann fits (z_{APP}) versus [Cu^{2+}].

The Mechanism of Cu^{2+} Action

Several different mechanisms could potentially account for a shift in the G_K-V relation by Cu^{2+}, including inhibition of either the closed to open conformational change or voltage sensor activation. To help distinguish among these possibilities we examined the effects of saturating 100 μM Cu^{2+} on steady-state open probability (P_O) over a wide voltage range in 0 or 5 μM intracellular

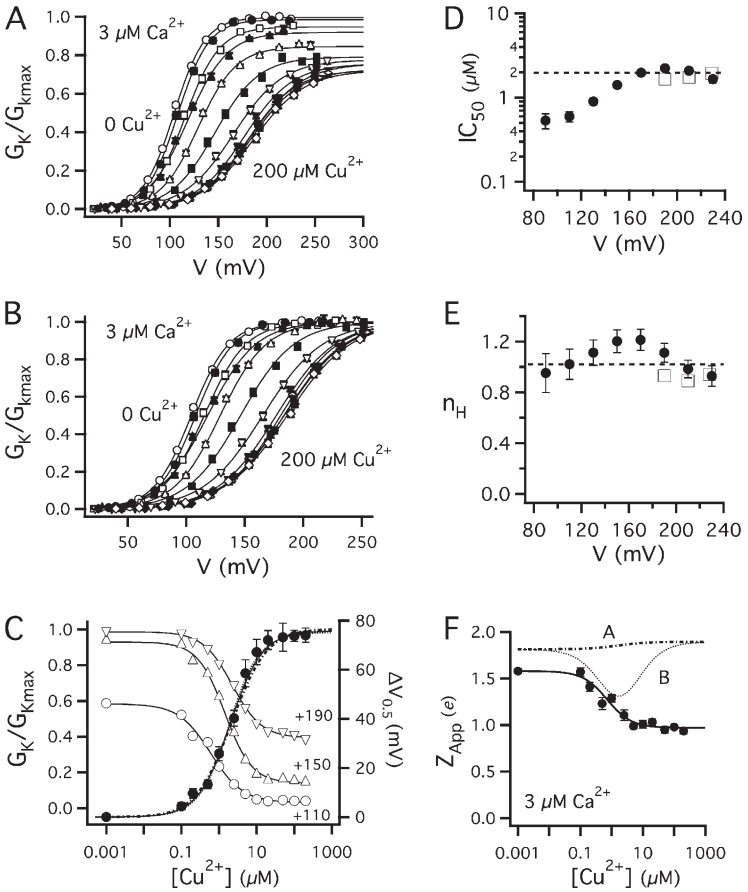

Figure 2. mSlo1 channels are extremely Cu^{2+} sensitive. (A) Mean G_K-V relations with $[Ca^{2+}]_i$ = 3 μM at different $[Cu^{2+}]$: 0 (○), 0.1 (●), 0.2 (□), 0.5(▲), 1.0 (△), 2.5 (■), 5 (▽), 10 (▼), 20 (◇), 50 (◆), 100 (◣) and 200 μM (◇), are normalized by G_{Kmax} in 0 Cu^{2+} and fit by Boltzmann functions. (B) Mean G_K-V relations from panel A are normalized by G_{Kmax} at each $[Cu^{2+}]$ based on Boltzmann fits. (C) Cu^{2+} dose–response relations for $\Delta V_{0.5} = (V_{0.5}\ [Cu^{2+}] - V_{0.5}[0])$ (●) and $G_K[Cu^{2+}]$ at 110 mV (○), 150 mV (△) and 190 mV (▽) were determined from fits in A. Solid lines are fits to a Hill equation. Thick dotted curve is a fit to Eq. 1 with most parameters set to previously determined values (z_J = 0.58 *e*, $L_0 = 10^{-6}$, z_L = 0.3 *e*, $K_D(Ca^{2+})$ = 11 μM, C = 8, D = 25, E = 2.4) (Horrigan and Aldrich, 2002). V_{hC} = 162 mV was adjusted to fit $V_{0.5}$ of the 0 Cu^{2+} control, and Cu^{2+}-dependent parameters (K_{Dcu} = 0.75 μM, E_{cu} = 0.124) were then varied to fit the $V_{0.5}$-$[Cu^{2+}]$ relation. Thin dotted curve is a fit to Eq. 2 with K_{Dcu} = 2.1 μM, E_{cu} = 0.129, and all other parameters the same as for Eq. 1. (D) IC_{50} and (E) n_H obtained by fitting G_K-$[Cu^{2+}]$ relations in 3 μM Ca^{2+} (●) and 0 Ca^{2+} (□) are plotted at different voltages. Dashed lines are IC_{50} = 1.97 μM, n_H = 1.01 from the $\Delta V_{0.5}$-$[Cu^{2+}]$ relation fit in panel C. (F) Apparent charge (Z_{app}) from Boltzmann G_K-V fits in A are plotted versus $[Cu^{2+}]$ and fit by a Hill equation (IC_{50} = 0.72 ± 0.12 μM, n_H = 1.1 ± 0.2). Curves A and B are the predictions of Eqs. 1 and 2, respectively, using parameters from C.

Ca^{2+} and plotted the results on a semi-log scale in Fig. 3 A. P_O was measured to values as low as $\sim 10^{-7}$ by recording unitary current activity in macropatches (see Materials and methods). The mean log(P_o)-V relations in Fig. 3 A reveal several important features of Cu^{2+} action and suggest that Cu^{2+} acts in large part to inhibit voltage sensor activation.

At extreme negative voltage, log(P_o) achieves a weakly voltage-dependent limiting slope (Fig. 3 A, dotted lines) because BK channels can open even when voltage sensors are not activated (Horrigan and Aldrich, 1999; Horrigan et al., 1999). At these voltages, P_o reflects the intrinsic stability of the gate and is increased almost 100-fold by 5 μM Ca^{2+} (Fig. 3 A), illustrating that Ca^{2+} acts independent of voltage sensor activation to stabilize the open conformation (Horrigan and Aldrich, 2002). By contrast, 100 μM Cu^{2+} has little or no effect on P_o at extreme negative voltages in the presence or absence of Ca^{2+}, implying that Cu^{2+} does not act either by stabilizing the closed conformation nor by interfering with Ca^{2+} action. Instead, Cu^{2+} reduces P_o in a voltage-dependent manner, with maximal effect at intermediate voltages. This response is unlikely to reflect an intrinsic voltage dependence to Cu^{2+} binding since if Cu^{2+} enters a binding site in the membrane electric field from the extracellular solution it should bind best at more negative voltages where the impact of Cu^{2+} on P_O is least. Therefore, the voltage dependence of Cu^{2+} action is likely to arise from interaction with the voltage sensor. The major effect of 100 μM Cu^{2+} can be approximated by shifting the log(P_o)–V relation along the voltage axis by +45 mV (Fig. 3 B), consistent with an inhibition of voltage sensor activation. This shift is less than the +74 mV shift in $V_{0.5}$ (Fig. 2 B) because Cu^{2+} also causes a slight reduction in the slope of the log(P_o)-V relation (Fig. 3 B).

Cu^{2+} Action Is State Dependent

Cu^{2+} could potentially inhibit voltage sensor activation by binding in a state-dependent manner to the voltage sensor to stabilize the resting conformation, similar to the proposed mechanism of Zn^{2+} action on squid K^+ channels (Gilly and Armstrong, 1982a). If so, then Cu^{2+} should interact better with the resting than the activated state. To test this hypothesis, we examined the effect on BK channel activation of applying Cu^{2+} at different membrane potentials (Fig. 3, C and D). I_K was recorded in response to brief test pulses to +120 mV before and after application of 100 μM Cu^{2+} (Fig. 3 C) with $[Ca^{2+}]_i$ = 5 μM. Cu^{2+} was applied during a 500-ms prepulse immediately preceding the second test pulse. When Cu^{2+} was applied at prepulse voltages (V_{PRE}) that do not activate the channel (−80 to +40 mV), the steady-state current recorded during the second test pulse (I_{P2}) in the

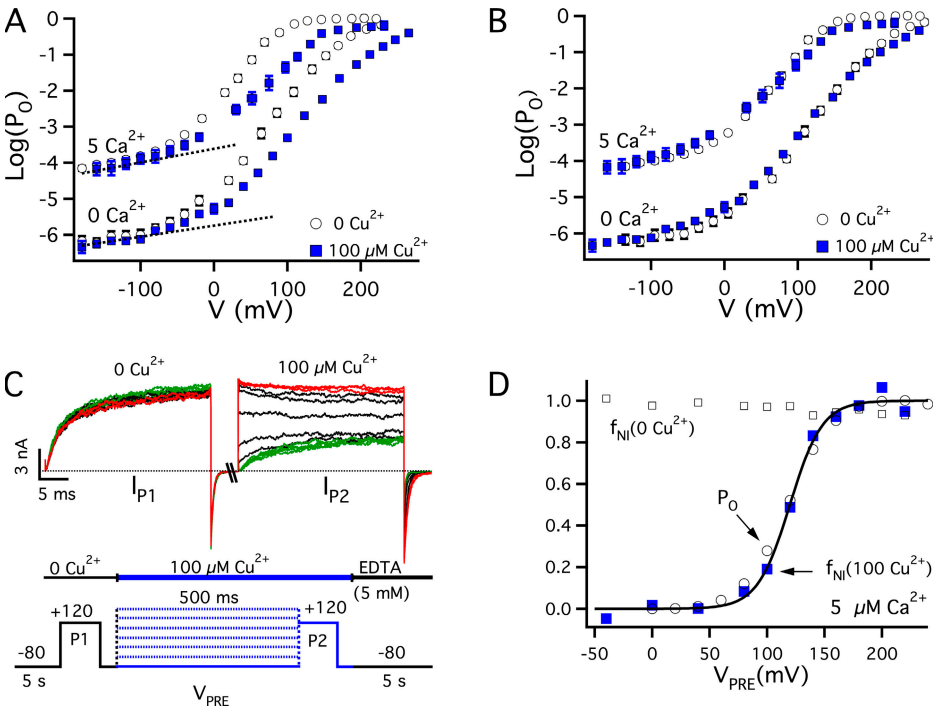

Figure 3. The mechanism and state dependence of Cu^{2+} action. (A) Mean log(P_o)-V relations for mSlo1 for 0 and 5 μM $[Ca^{2+}]_i$ in 0 Cu^{2+}(○) and 100 μM Cu^{2+}(■), respectively. Dotted lines are exponential fits to the limiting slope of log(P_o) with partial charge z_L = 0.3 *e*. (B) Log(P_o)-V relations from A are superimposed by shifting the 0 Cu^{2+} curves along the voltage axis by +45 mV. (C) I_K evoked by 30-ms test pulses to +120 mV before (I_{P1}) and after (I_{P2}) application of 100 μM Cu^{2+} using the illustrated protocol (5 μM $[Ca^{2+}]_i$), without leak subtraction. I_{P1} was evoked from a holding potential of −80 mV in 0 Cu^{2+} following perfusion with standard external solution for 5 s. I_{P2} was recorded in 100 μM Cu^{2+} following perfusion with 100 μM Cu^{2+} for 500 ms at different prepulse voltages (V_{PRE}). Following the second pulse the patch was washed at −80 mV for 5 s with 5 mM EGTA and then for 5 s with standard external solution before repeating the protocol. Maximal inhibition of I_{P2} was observed with V_{PRE} = −80 to +40 mV (green traces) and minimal inhibition with V_{PRE} = +180 to +220 mV (red traces). (D) The fraction of channels not inhibited $f_{NI} = (I_{P2}[V_{PRE}] - I_{P2}[-80])/(I_{P1} - I_{P2}[-80])$ from C (■, f_{NI}[100 Cu^{2+}]) is plotted against V_{PRE} and compared with the mean steady-state P_o-V relation (○) in 0 Cu^{2+} and 5 μM $[Ca^{2+}]_i$ estimated as G_K/G_{Kmax}. A control experiment (□, f_{NI}[0 Cu^{2+}]) obtained from a different patch using the pulse protocol in C shows that f_{NI} is voltage independent when the 100 μM Cu^{2+} solution is replaced with 0 Cu^{2+}.

presence of Cu^{2+} was reduced to ∼40% of the control (I_{P1}) (Fig. 3 C, green traces). However, at more depolarized V_{PRE} the inhibitory effect of 100 μM Cu^{2+} was reduced, and no difference between I_{P1} and I_{P2} was observed at $V_{PRE} \geq +180$ mV (Fig. 3 C, red traces). The dependence of Cu^{2+} inhibition on prepulse voltage was analyzed by estimating the fraction of channels not inhibited as $f_{NI} = (I_{P2}[V_{PRE}] - I_{P2}[-80])/(I_{P1} - I_{P2}[-80])$ and plotting this quantity versus V_{PRE} (f_{NI}[100 Cu^{2+}], Fig. 3 D). These data superimpose on the mean P_o-V relation obtained in 0 Cu^{2+} (P_O, Fig. 3 D), suggesting that Cu^{2+} interacts poorly and/or is poorly accessible to its binding site when channels are activated. Indeed the failure of traces in Fig. 3 C to converge to the same current level at the end of the second test pulse suggests that Cu^{2+} binding does not equilibrate within 30 ms at the test pulse condition (+120 mV, 100 μM Cu^{2+}), favoring the possibility that access of Cu^{2+} to its binding site is slow in the activated channel.

It should be noted that the results in Fig. 3 (C and D) do not distinguish whether the state dependence of Cu^{2+} action reflects a failure to interact with the activated voltage sensor or the open conformation. In BK channels the voltage dependence of voltage sensor activation (Q-V relation) and P_o-V relation differ in 0 Ca^{2+} but are superimposable in saturating 70 μM Ca^{2+} (Horrigan and Aldrich, 2002). We did not measure the Q-V relation under the experimental conditions in Fig. 3 C (5 μM Ca^{2+}). However, an allosteric gating scheme that reproduces the 0 and 70 μM Ca^{2+} data (Horrigan and Aldrich, 2002) predicts the half-activation voltages of Q-V and P_O-V in 5 μM $[Ca^{2+}]$ should differ by only 3 mV. Thus the similar voltage dependence of f_{NI}[100 Cu^{2+}] and P_O in Fig. 3 D is compatible with a dependence of Cu^{2+} inhibition on either channel opening or voltage sensor activation.

BK Channel Inhibition Is Cu^{2+} Selective

To further characterize the metal sensitivity of mSlo1, we compared the effect on $V_{0.5}$ of different transition metals (Cu^{2+}, Zn^{2+}, Fe^{3+}, Mn^{2+}, Ni^{2+}, Co^{2+}, and Cd^{2+}) at 100 μM (Fig. 4 A). Cu^{2+} produced by far the greatest shift in $V_{0.5}$ (+74.3 ± 2.7 mV), followed by Cd^{2+} (+19.0 ± 1.9 mV) and Zn^{2+} (+8.5 ± 1.5 mV). None of the other metals tested significantly altered $V_{0.5}$. These results indicate that, among the metals tested, the BK channel is primarily sensitive to Cu^{2+} at physiologically relevant concentrations.

The weak response of mSlo1 to metals other than Cu^{2+} at 100 μM suggests either that these metals bind to the channel with much lower affinity than Cu^{2+}, or their occupancy of the binding site has little effect on gating. To distinguish these possibilities we examined the response to higher metal concentrations (Fig. 4, B and C). As Cd^{2+} was increased beyond 100 μM, G_K-V relations

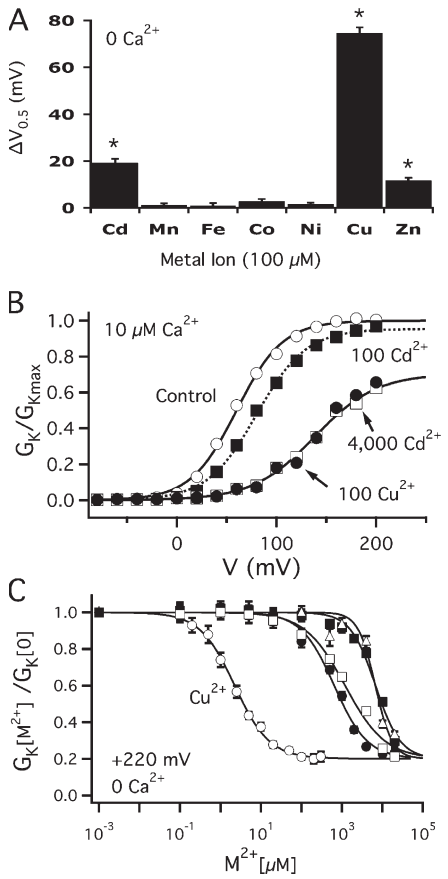

Figure 4. Cu^{2+} selectively inhibits mSlo1 activation. (A) G_K-V shift ($\Delta V_{0.5}$) produced by 100 μM of different transition metals (Cd^{2+}, Mn^{2+}, Fe^{3+}, Co^{2+}, Ni^{2+}, Cu^{2+}, Zn^{2+}) (0 $[Ca^{2+}]_i$). Stars indicate a significant change in $V_{0.5}$ relative to the control ($P < 0.05$, paired *t* test). (B) G_K-V relations in the absence of metal ions (○), 100 μM Cu^{2+} (●), 100 μM Cd^{2+} (■), or 4,000 μM Cd^{2+} (□) were normalized by the control and fit with Boltzmann functions (10 μM $[Ca^{2+}]_i$). (C) Dose–response relations for inhibition of G_K[+220 mV] by different metal ions (0 $[Ca^{2+}]_i$) fit with Hill equations (Cu^{2+} (○) IC_{50} = 2.0 μM, n_H = 0.98; Cd^{2+} (●) IC_{50} = 0.70 mM, n_H = 1.0; Zn^{2+} (□) IC_{50} = 1.2 mM, n_H = 0.87; Mn^{2+} (■) IC_{50} = 6.7 mM, n_H = 1.4; Ni^{2+} (△) IC_{50} = 7.8 mM, n_H = 1.5).

continued to shift to more positive voltages, producing a response in 4000 μM Cd^{2+} similar to that of 100 μM Cu^{2+} (Fig. 4 B). Thus Cd^{2+} can alter gating to the same extent as Cu^{2+}, but at much higher concentrations. The dose–response relation for Cd^{2+} is similar in shape to that of Cu^{2+} but characterized by an IC_{50} of 0.70 mM (Fig. 4 C). This IC_{50} may be overestimated by approximately twofold owing to the ability of Cd^{2+} to complex with chloride (see Materials and methods), but is still more than two orders of magnitude greater than the IC_{50} of Cu^{2+}. Partial dose–response relations were also obtained for Zn^{2+} (IC_{50} = 1.2 mM), Mn^{2+}, and Ni^{2+} (Fig. 4 C), indicating that these metals are also capable of inhibiting BK channel activation at much higher concentrations than Cu^{2+}. Therefore the metal binding site appears to be highly selective for Cu^{2+}.

The dose–response curves for Mn^{2+} and Ni^{2+} in Fig. 4 C are steeper than those of Cu^{2+}, Cd^{2+}, or Zn^{2+}, possibly reflecting a different site or mechanism of action or an additional contribution to G_K inhibition from surface charge screening at millimolar concentrations. Charge screening has little effect on BK channel activation in neutral bilayers (MacKinnon et al., 1989), and is estimated in cell membranes to shift $V_{0.5}$ by only ~3 mV in response to an increase in divalent cation concentration from 1 to 10 mM, and ~9 mV from 10 to 100 mM (Hu et al., 2006). Thus, surface charge effects should be small compared with the 75-mV G-V shift caused by Cu^{2+} and can only account for a fraction of the G_K decrease by Mn^{2+} and Ni^{2+}.

The Cu^{2+} Binding Site Does Not Include Cys or His

To locate the Cu^{2+} binding site we mutated individual amino acid residues to identify those that influence the IC_{50} for Cu^{2+}. Any side chain containing oxygen, nitrogen, or sulfur atoms can potentially interact with metal ions. However Cys and His are by far the most common coordinating residues in transition metal binding sites (Rulisek and Vondrasek, 1998). mSlo1 contains three Cys (C14, C141, and C277) and one His (H254) that are potentially accessible to the extracellular solution. A triple mutant lacking all three Cys (C14A/C141A/C277A) exhibited a G_K-V relation and inhibition by 100 μM Cu^{2+} similar to the WT (Fig. 5 A). Likewise, H254A shifted the G_K-V by approximately +60 mV but exhibited a similar $V_{0.5}$ shift as the WT in response to 100 μM Cu^{2+} (Fig. 5 B). Dose–response relationships for H254A and C14A/C141A/C277A were indistinguishable from the WT (Fig. 5 C). Therefore, we conclude that native Cys and His residues do not participate in Cu^{2+} binding.

Cu^{2+} Action Is pH Dependent

Acidic amino acids (Asp and Glu) are often important in coordinating metal ions. To test for the participation of such groups in Cu^{2+} binding, we examined the ability of 100 μM Cu^{2+} to inhibit G_K at different extracellular pH (Fig. 5 D). The reduction in G_K at +220 mV was maximal from pH 7.2 to 8.2, but inhibition was relieved under more acidic conditions and almost eliminated at the lowest pH tested (5.2). This relief of inhibition was not due to a change in channel gating because reducing pH from 7.2 to 5.2 produced only a small +20-mV shift in $V_{0.5}$. Thus the effect of pH on Cu^{2+} action likely reflects a decrease in Cu^{2+} binding at acidic pH.

The pH dependence of 100 μM Cu^{2+} action was fit by a Hill equation (Fig. 5 D, solid line) with half-relief of inhibition at pH 6.0 (n_H = 1.1), suggesting Cu^{2+} is coordinated by one or more protonatable side chains with a pKa near 6. Since we have already ruled out the participation of histidine, this suggests that acidic residues may be involved. Although the mean pKa values for Asp and Glu in proteins are 3.4 and 4.1, respectively, values

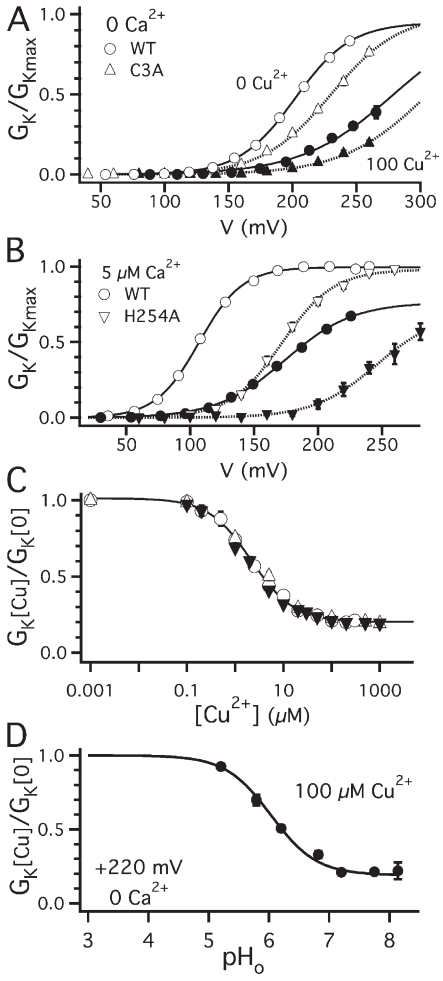

Figure 5. Cu^{2+} action is independent of native Cys and His residues but is pH dependent. (A) G_K-V relations for WT (○: 0 Cu^{2+}; ●: 100 Cu^{2+}) and C14A/C141A/C277A ("C3A", △: 0 Cu^{2+}; ▲: 100 Cu^{2+}) show similar inhibition by 100 μM Cu^{2+}. (B) G_K-V relations for WT (○: 0 Cu^{2+}; ●: 100 Cu^{2+}) and H254A (▽: 0 Cu^{2+}; ▼: 100 Cu^{2+}) also respond similarly to 100 μM Cu^{2+} as indicated by the shift in $V_{0.5}$. (C) Mean dose–response relations (G_K-$[Cu]^{2+}$) measured at voltages near $V_{0.5}$ for WT (○), C14A/C141A/C277A (△), and H254A (▼) are indistinguishable. The solid line is a fit by the Hill equation (IC_{50} = 2.0 μM, n_H = 0.98) (D) Dependence of Cu^{2+} action on extracellular pH (pH_O) is fit by Hill equation ($pH_{0.5}$ = 6.0, n_H = 1.15). G_K-pH_O relation for WT channels at +220 mV in 0 Ca^{2+} represents G_K in 100 μM Cu^{2+} normalized by G_K in 0 Cu^{2+} at each pH_O.

>6 have been reported, usually in enzyme active sites and ligand-binding sites (Forsyth et al., 2002).

An Acidic Residue in S2 Contributes to Cu^{2+} Sensitivity

To identify acidic residues that coordinate Cu^{2+} we focused initially on the S2 and S3 segments of the voltage sensor domain because acidic residues in these segments of dEAG and hERG channels have been implicated in metal binding. An amino acid sequence alignment of dEAG and hERG with mSlo1 and several other voltage-dependent channels (Fig. 6 A) illustrates that dEAG and hERG contain an unusually large number of acidic residues in S2 and S3, three of which (boxed) contribute to divalent cation sensitivity (Silverman et al., 2004; Fernandez et al., 2005). Only one of these putative coordinating residues is conserved in other Kv channels, corresponding to D153 in the S2 segment of mSlo1. Mutation of D153 in mSlo1 greatly alters the dose–response curve for Cu^{2+} (Fig. 6 B). Substitution of Lys at this position (D153K) reduced Cu^{2+} sensitivity (increasing IC_{50} eightfold to 15.9 μM), whereas a His increased Cu^{2+} sensitivity (decreasing IC_{50} eightfold to 0.26 μM). In both cases, mutant dose–response curves were shifted relative to the WT (dotted curve) with little change in shape, consistent with a change in the affinity of a single binding site. Thus D153 in S2 appears to contribute to Cu^{2+} binding in BK channels.

Identification of Cu^{2+} Coordinating Residues

Fig. 6 B illustrates two important principals that we used to identify potential Cu^{2+}-coordinating sites. First, we measured dose–response curves for each mutant to obtain a quantitative indication of changes in Cu^{2+} sensitivity (IC_{50}), related to binding affinity. Measurements at a single Cu^{2+} concentration cannot distinguish changes in affinity from changes in efficacy; and efficacy can in principal be altered by modifications in gating that are not directly related to Cu^{2+} binding. We also measured IC_{50} because we do not expect single mutations to abolish Cu^{2+} binding in an all or none fashion. The high sensitivity and selectivity of mSlo1 for Cu^{2+} suggests that Cu^{2+} may be coordinated by multiple residues, no one of which is critical for binding. In metalloprotein and small molecule binding sites of known structure, Cu^{2+} is usually coordinated by three to eight groups (Rulisek and Vondrasek, 1998). Second, at each site we compared the effects of multiple mutations, including those expected to inhibit or enhance binding. A correlation between changes in IC_{50} and the expected ability of different side chains to interact with metals, as in Fig. 6 B, provides support that a candidate position interacts directly with Cu^{2+}. The use of multiple substitutions also helped to control for effects of mutation on channel gating. Mutations in the voltage sensor often shift or alter the shape of the G_K-V relation (Ma et al., 2006). We controlled for G_K-V shifts to some extent by measuring dose–response curves for all mutants at their $V_{0.5}$ (Table I); and small shifts are not expected to greatly effect IC_{50} determination since similar values were obtained for the WT at different voltages (Fig. 2 C). However, because Cu^{2+} action is state dependent (Fig. 3, C and D), large changes in channel gating can potentially influence IC_{50}. Therefore, when possible, we compared mutants at each site that exhibit very similar gating properties. One such case is D153, which has previously been identified as contributing to gating charge in mSlo1 (Ma et al., 2006). The mutations at this site substantially reduce gating charge and shift $V_{0.5}$ to more positive voltages, but the

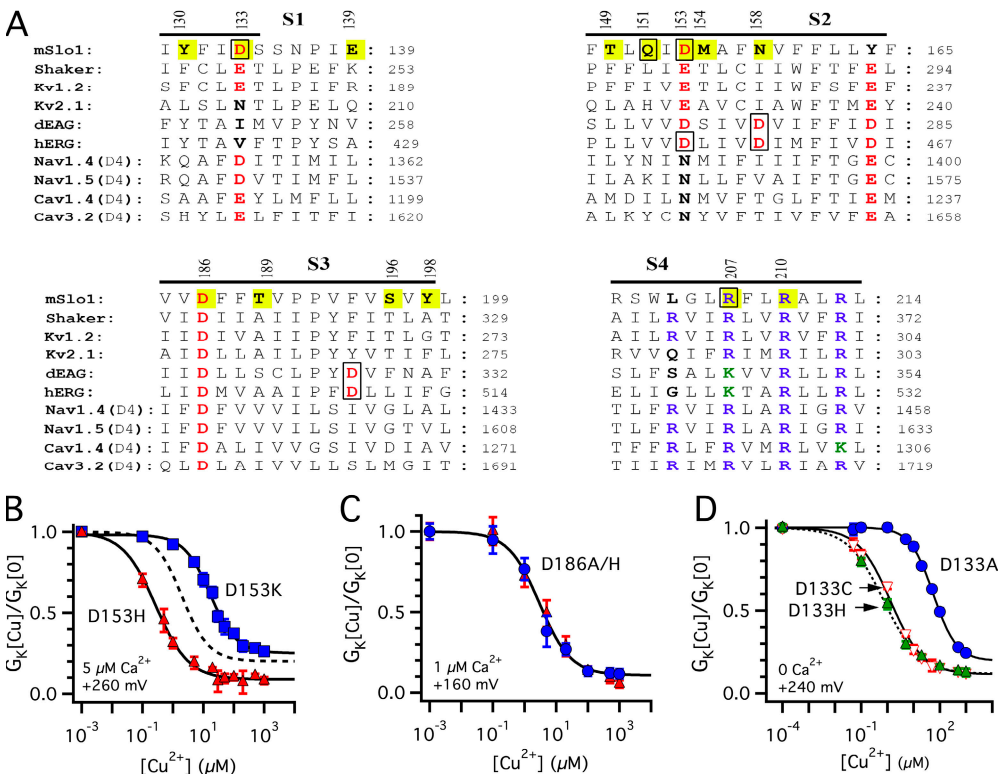

Figure 6. Acidic residues contribute to metal sensitivity of mSlo1 and other voltage-gated channels. (A) Multiple sequence alignment of voltage sensor domain from mSlo1, Kv channels (Shaker, Kv1.2, and Kv2.1), dEAG, and hERG, and other voltage-gated channels (Nav1.4, Nav1.5, Cav1.4, Cav3.2 Domain IV) (based on Liu et al., 2003; Long et al., 2007). Putative transmembrane segments are indicated by solid bars (Long et al., 2007). Charged residues that are highly conserved in mSlo1 and other voltage-gated channels are in red (acidic) or blue (basic). Sites that were mutated in mSlo1 are highlighted yellow with positions labeled. Putative metal coordinating residues in mSlo1, dERG, and hERG are indicated by boxes. (B) Dose–response relations (G_K at +260 mV) fit by Hill equations for D153K (■, IC_{50} = 16.7 μM, n_H = 1.0) and D153H (▲, IC_{50} = 0.26 μM, n_H = 0.73) (5 μM $[Ca^{2+}]_i$). Dashed curve represents fit to WT data from Fig. 5 C. (C) The dose–response relation (G_K at +160 mV) for D186A (●, IC_{50} = 2.53 μM, n_H = 0.97), D186H (▲, IC_{50} = 2.82 μM, n_H = 0.95) (1 μM $[Ca^{2+}]_i$). (D) The dose–response relations (G_K at +240 mV) for D133A (●, IC_{50} = 56.5 μM, n_H = 0.97), D133C (▽, IC_{50} = 1.5 μM, n_H = 0.74) and D133H (▲, IC_{50} = 0.73 μM, n_H = 0.63) (0 $[Ca^{2+}]_i$).

mutants in Fig. 6 B (D153K and D153H) have similar G_K-V properties as indicated by Boltzman fit parameters in Table I.

An Acidic Residue in S1 also Contributes to Cu^{2+} Sensitivity

Although D153K substantially increased IC_{50}, it only slightly reduced the ability of 100 μM Cu^{2+} to inhibit G_K (Fig. 6 B), and therefore does not recapitulate the response of the WT to low pH. This suggests that additional acidic residues may be present in the Cu^{2+} binding site. mSlo1 contains a highly conserved Asp in S3 (D186) (Fig. 6 A). Mutation of D186 to Ala in mSlo1 has substantial effects on channel gating (Ma et al., 2006). However, D186A and D186H have similar gating properties (Table I) and indistinguishable dose–response curves (Fig. 6 C), implying that D186 is not involved in Cu^{2+} binding.

The only other acidic residue in the S1–S4 segments of mSlo1 that is potentially accessible to Cu^{2+} is D133, at the extracellular end of S1. This position is highly conserved in most voltage-gated channels (Fig. 6 A), and the residues equivalent to D133 and D153 contact each other in the crystal structure of Kv1.2 (Long et al., 2005b), suggesting a likely role for D133 in Cu^{2+} binding. Consistent with this prediction, D133A increased IC_{50} almost 30-fold relative to the WT, whereas D133C and D133H decreased IC_{50} 1.4- and 3-fold (Fig. 6 D). Mutations at this site have similar small effects on gating (Table I) (Ma et al., 2006), supporting a direct role for D133 in Cu^{2+} binding.

Contribution of Nonacidic Residues to Cu^{2+} Sensitivity

To further characterize the Cu^{2+}-binding site, we mutated 10 additional positions in S1–S4 segments plus E139 in the S1–S2 linker (Fig. 6 A). We tested all potential metal-coordinating residues in transmembrane segments that are close to D133 or D153 based on primary sequence and the structure of Kv1.2, as well as loci in S2 or S3 that interact with metals in dEAG and hERG. The effects of different mutations on the IC_{50} for Cu^{2+} are summarized in Fig. 7 A.

We attempted to inhibit Cu^{2+} binding by substituting Ala at each position (Fig. 7 A, open circles). In a few positions (D153, R207, and R210) where Ala mutations failed to express functional channels or expressed poorly, alternative "low-affinity" substitutions were used (Lys, Gln, and Asn). In many cases, mutants exhibited IC_{50}s indistinguishable from the WT (dotted line). At all positions tested in S1–S4 segments we also made "high-affinity" substitutions (His or Cys) in an attempt to enhance Cu^{2+} sensitivity. A total of six positions were identified

TABLE I

Boltzmann Fit Parameters for mSlo1 G_K-V Relations

Segments	Channel	$V_{0.5}$ (mV)	Z_{APP} (e)	n	$[Ca^{2+}]_i$
	WT	206.50 ± 3.81	1.01 ± 0.050	8	0
Native Cys and His	C14A/C277A	234.18 ± 3.55	0.96 ± 0.028	6	0
	C141A/C277A	230.22 ± 2.97	0.94 ± 0.011	7	0
	C14A/C141C/C277A	237.91 ± 3.53	0.95 ± 0.049	7	0
	H254A	169.08 ± 3.23	1.24 ± 0.044	7	5
S1	Y130A	202.02 ± 4.31	0.64 ± 0.022	8	0
	Y130H	216.66 ± 3.37	0.85 ± 0.059	6	0
	D133A	229.72 ± 2.31	1.01 ± 0.023	19	0
	D133C	238.21 ± 1.48	1.08 ± 0.023	17	0
	D133H	224.15 ± 1.56	1.04 ± 0.026	14	0
S2	T149C	202.47 ± 2.48	0.93 ± 0.029	5	0
	Q151A	230.56 ± 3.01	0.96 ± 0.030	13	0
	Q151C	230.56 ± 2.72	0.99 ± 0.022	18	0
	Q151H	229.60 ± 3.71	0.98 ± 0.029	12	0
	D153K	201.96 ± 3.22	0.84 ± 0.030	23	50
	D153H	207.79 ± 3.99	0.84 ± 0.034	6	50
	M154A	200.39 ± 3.10	0.96 ± 0.027	7	0
	M154C	201.62 ± 4.62	0.84 ± 0.023	5	0
	N158A	197.61 ± 2.89	0.81 ± 0.015	4	0
	N158C	196.03 ± 4.18	0.83 ± 0.019	4	0
S3	D186A	148.92 ± 2.98	0.95 ± 0.051	5	1
	D186H	144.55 ± 2.58	0.97 ± 0.032	6	1
	T189A	232.94 ± 5.49	0.95 ± 0.026	4	0
	T189C	231.51 ± 2.58	1.10 ± 0.047	3	0
	S196A	212.36 ± 1.77	0.95 ± 0.026	5	0
	S196C	213.70 ± 2.67	0.98 ± 0.030	4	0
	Y198A	213.05 ± 4.32	0.83 ± 0.017	6	0
	Y198C	216.88 ± 3.10	0.89 ± 0.030	7	0
S4	R207Q	149.66 ± 2.34	0.62 ± 0.016	8	0
	R207C	147.85 ± 2.90	0.61 ± 0.017	10	0
	R210N	158.12 ± 6.96	0.60 ± 0.019	6	1
	R210C	158.47 ± 5.97	0.55 ± 0.028	9	0

where low-affinity substitutions increased IC_{50}, but only four of these showed a difference in IC_{50} between low- and high-affinity substitutions, indicated by vertical bars in Fig. 7 A. In addition to D133 and D153, these putative Cu^{2+}-coordinating sites are Q151 in S2 (Fig. 7 B) and R207 in S4 (Fig. 7 C). Two sites (R210 and Y130) showed decreases in Cu^{2+} sensitivity independent of the substituting residue. In the case of R210, this is likely to reflect an effect of mutation on gating as discussed below. Y130 could conceivably act as an electron-withdrawing group to enhance interaction of Cu^{2+} with the putative coordinating residue D133 located one helical turn away.

Altering the Selectivity of Metal Binding

Substitution of putative Cu^{2+}-coordinating sites with Cys or His produced a substantial eightfold increase in Cu^{2+} sensitivity in the case of D153H, but a more modest 1.4–4-fold increase at positions 133, 151, and 207 (Fig. 7 A). Such a result is not unexpected because Cu^{2+} is not strongly selective for Cys or His over other side chains. However, to confirm that D133, Q151, and R207 participate directly in metal coordination we also looked at their Cd^{2+} sensitivity. Cd^{2+} interacts strongly with Cys or His, therefore Cys or His substitutions should have a much greater effect on the sensitivity of the channel for Cd^{2+} than Cu^{2+}. Consistent with this prediction, D133C, Q151H, and R207C mutations produced more than 1,000-fold decreases in the IC_{50} for Cd^{2+} relative to the WT (Fig. 7 A, filled symbols). Indeed, these mutants were all more sensitive to Cd^{2+} than Cu^{2+}. The ability of Cys or His substitutions to enhance Cd^{2+} sensitivity and switch the selectivity of the channel for Cd^{2+} versus Cu^{2+} supports that D133, Q151, and R207 participate directly in metal binding.

The Role of R207 in Cu^{2+} Sensitivity

The identification of R207 in S4 as a potential Cu^{2+}-coordinating residue is notable because this site plays an important role in voltage sensor activation (Ma et al., 2006) and because the presence of arginine in metal

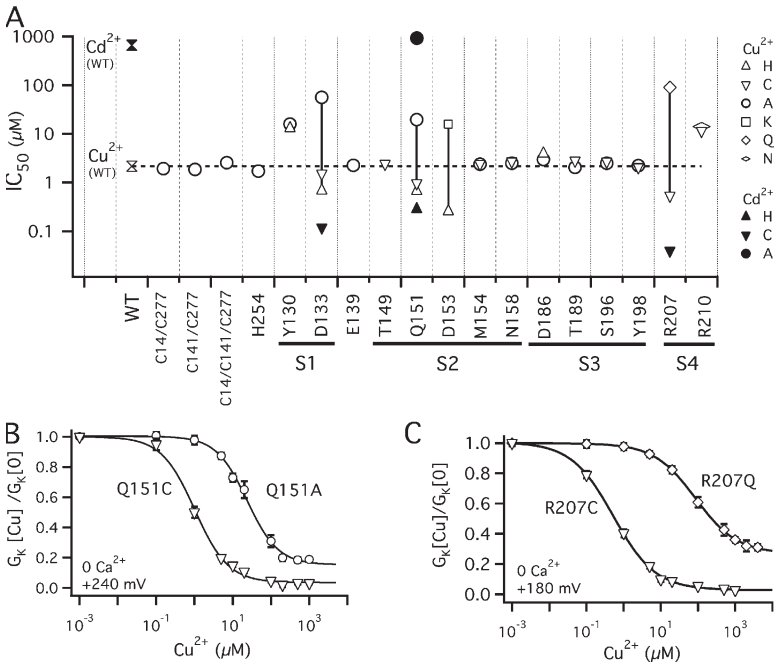

Figure 7. Nonacidic residues also contribute to Cu^{2+} sensitivity. (A) IC_{50}s of mutant channels are plotted at each position tested for Cu^{2+} (open symbols) or Cd^{2+} (filled symbols). Error bars were within the symbol size and therefore excluded. Symbols indicate different substitutions (WT: ⧖, ⧗; Ala: ○, ●; Lys: □; Gln: ◇; Asn: ◇; Cys: ▽,▼; His: △, ▲). Dashed line indicates the IC_{50} of the WT for Cu^{2+}. Vertical solid lines indicate the differences in IC_{50} between mutants at putative coordination sites. Dose–response relations (G_K-[Cu^{2+}]) for putative coordination sites 151 and 207 in 0 Ca^{2+} are plotted and fit by Hill equations in (B) Q151A (○, IC_{50} = 23.8 μM, n_H =1.0), Q151C (▽, IC_{50} = 0.96 μM, n_H = 0.97) at +240 mV and (C) R207Q (◇, IC_{50} = 85.8 μM, n_H = 0.77) and R207C (▽, IC_{50} = 0.52 μM, n_H = 0.77) at +180 mV.

binding sites is rare. Therefore we investigated the contribution of R207 in more detail (Fig. 8).

The participation in metal binding of the Arg side chain, which is protonated and therefore positively charged at physiological pH, is unusual but not unprecedented (Bewley et al., 1999; Ferraroni et al., 2002; Berkovitch et al., 2004; Di Costanzo et al., 2006). Unlike Lys, the Arg side chain is bifurcated such that the proton is delocalized and two nitrogens are potentially available to interact with a metal ion. Nevertheless, two issues must be addressed to confirm the involvement of R207 in Cu^{2+} binding. First, the possibility that differences in IC_{50} among mutant and WT channels reflect differences in gating rather than Cu^{2+} binding is of particular concern in the case of R207. Mutations of this site greatly facilitate voltage sensor activation (Ma et al., 2006), which could reduce Cu^{2+} sensitivity, given the state dependence of Cu^{2+} action (Fig. 3, C and D). Second, our analysis assumes that changes in IC_{50} reflect modification of a native binding site; but the possibility must also be considered for any putative coordinating residue that high-affinity (Cys and His) substitutions modify Cu^{2+} sensitivity by introducing a new binding site.

The R207Q mutation shifts voltage sensor activation (i.e., the Q-V relation) to more negative voltages by >200 mV (Ma et al., 2006), such that the P_o-V relation for R207Q in 0 Cu^{2+} (Fig. 8 A) is left shifted and shallow compared with the WT (Table I). The possibility that this change in gating contributes to the increased IC_{50} of R207Q relative to the WT is supported by the observation that mutations at position 210 (R210N and R210C), which also enhance voltage sensor activation (Ma et al., 2006), exhibit a P_o-V similar to R207Q (Table I) and increase IC_{50} (Fig. 7 A). Thus the reduced Cu^{2+} sensitivity of R207Q cannot be taken as conclusive evidence that an Arg at this position normally interacts with Cu^{2+}. That said, R207 is clearly in a position to interact with Cu^{2+} because the steady-state activation of R207Q and R207C are almost identical in the absence of Cu^{2+} (Fig. 8 A), implying that the 170-fold difference in IC_{50} for these mutants (Fig. 7 A) must reflect a difference in Cu^{2+} binding rather than gating.

The assumption that R207 mutations modify a native binding site is supported by the dose–response relations of these mutants for Cu^{2+} (Fig. 7 C) or Cd^{2+} (Fig. 8 C). If a mutation enhances metal sensitivity by introducing a new binding site with effects on gating independent of the native site, then the mutant should exhibit a biphasic dose–response relation. In no case was this observed. For all four putative coordinating sites, Cu^{2+} dose–response relations were shifted by mutation with little change in shape and were well fit by Hill equations with n_H near 1. The G_K-[Cu^{2+}] relations for R207Q and R207C at +180 mV were best fit by Hill coefficients of 0.75 ± 0.03 and 0.77 ± 0.07, respectively (Fig. 7 C). Similarly, R207C decreases the IC_{50} for Cd^{2+} by more than four orders of magnitude relative to the WT (Fig. 7 A) with little effect on the shape of the dose–response curve (Fig. 8 C). Thus, the dose–response of R207C appears monotonic and saturated over the concentration range where R207Q or the WT respond to Cu^{2+} or Cd^{2+}, respectively, consistent with modification of a single binding site. It is conceivable that a second phase of inhibition for R207C might exist at concentrations >100 μM but be difficult to detect from the dose–response curve because G_K at +180 mV is already reduced by >90% in 100 μM Cu^{2+} or Cd^{2+}. However, we can show that this is not the case by comparing G_K-V relations for R207C in 100 and 1000 μM

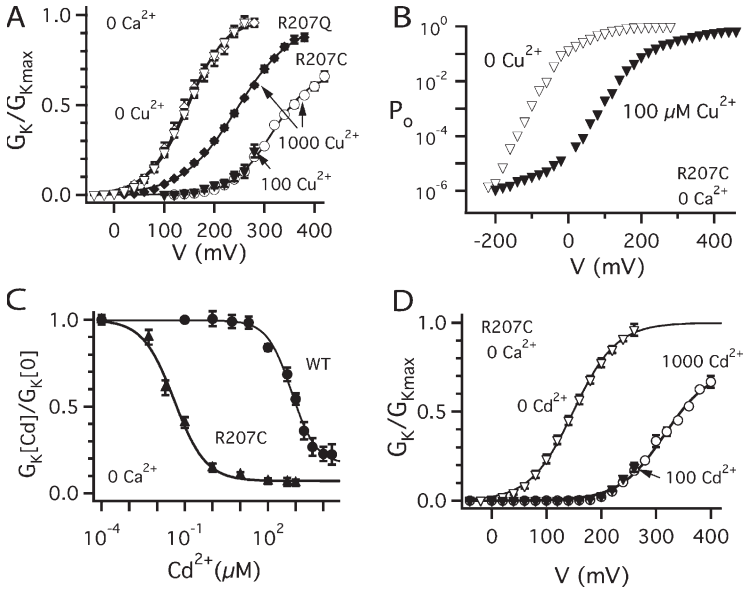

Figure 8. The role of R207 in Cu^{2+} sensitivity. (A) G_K-V relations fit by Boltzmann functions for R207C (◇) and R207Q (▽) in 0 Cu^{2+} ($V_{0.5}$ = 149 mV, z_{APP} = 0.64 *e*) and in 100 μM Cu^{2+} (R207C, ▼) and 1000 μM Cu^{2+} (R207C: ○, $V_{0.5}$ = 314.5 mV, z_{APP} = 0.64 *e*; R207Q: ◆, $V_{0.5}$ = 245.6 mV, z_{APP} = 0.46 *e*). (B) Log(P_o)-V relation for R207C in 0 (▽) and 100 μM Cu^{2+} (▼). (C) Cd^{2+} dose–response relations (G_K-[Cd^{2+}]) fit by Hill equations for WT (●, IC_{50} = 720 μM, n_H = 0.98) at +220 mV and R207C (▲, IC_{50} = 0.038 μM, n_H = 0.73) at +180 mV (0 [Ca^{2+}]$_i$). (D) G_K-V relations for R207C in 0 Cd^{2+} (▽, $V_{0.5}$ = 149 mV, z_{APP} = 0.64 *e*), 100 μM Cd^{2+} (▼), and 1000 μM Cd^{2+} (○, $V_{0.5}$ = 316 mV, z_{APP} = 0.61 *e*) (0 [Ca^{2+}]$_i$).

Cu^{2+} (Fig. 8 A) or Cd^{2+} (Fig. 8 D). In both cases there is no appreciable change in the G_K-V relation over this concentration range, indicating that the response of R207C is indeed saturated at 100 μM Cu^{2+} or Cd^{2+}.

Effects of Voltage Sensor Mutations on Cu^{2+} Efficacy

If Cu^{2+} inhibits BK channel activation by binding in a state-dependent manner to the voltage sensor, then mutations in the binding site may alter not only IC_{50} but also efficacy. Efficacy can be defined as the extent to which a saturating concentration of Cu^{2+} shifts the G_K-V relation ($\Delta V_{0.5MAX}$), and is ultimately determined by the relative affinity (i.e., K_ds) of Cu^{2+} for different states (Colquhoun, 1998).

Why do we expect mutations to alter efficacy, and what do such effects reveal about the interaction of Cu^{2+} with coordinating residues? If Cu^{2+} binds in a state-dependent manner then the sum its energetic interactions with coordinating groups must be state dependent. Thus Cu^{2+} interaction with some individual coordinating groups must be state dependent while others may be state independent. Mutations of a state-dependent group that presumably abolish interaction with Cu^{2+}, such as the substitution of a coordinating residue by Ala, must alter Cu^{2+} efficacy because a state-dependent component of the net binding energy will be eliminated. Mutations that enhance interaction with Cu^{2+} are also likely to alter efficacy, but are not certain to do so unless the site only interacts with Cu^{2+} in a single state such as the resting state. By contrast, Ala substitution at a state-independent site should reduce apparent affinity (increase IC_{50}) without altering efficacy, a so-called pure binding effect (Colquhoun, 1998). A high-affinity substitution at such a site is also likely but not certain to leave efficacy unchanged unless coordination geometry is identical in different states.

The effects of mutation on Cu^{2+} efficacy for mSlo1 (Fig. 9 A) suggest that some cooridinating residues interact with Cu^{2+} in a state-dependent manner while others do not. Fig. 9 A plots $\Delta V_{0.5MAX}$ measured with saturating 1000 μM Cu^{2+} for various mutations of the four putative Cu^{2+}-coordinating sites. Mutations in S2 (Q151, D153) that alter IC_{50} (Fig. 7 A) have no effect on efficacy (Fig. 9 A), suggesting that S2 interacts with Cu^{2+} in a state-independent manner. By contrast, mutation of R207 (S4) or D133 (S1) had effects on efficacy that parallel their impact on IC_{50} (Fig. 7 A). That is, mutations that increased apparent affinity (decreasing IC_{50}) also increased $\Delta V_{0.5MAX}$, suggesting that D133 and R207 interact with Cu^{2+} in a state-dependent manner. Although the magnitude of $\Delta V_{0.5MAX}$ can potentially be influenced by the steepness of the G_K-V relation (Cui and Aldrich, 2000), mutants tested at each site had similar G_K-V shapes (Table I, Fig. 8 A), implying that variations in $\Delta V_{0.5MAX}$ do not reflect effects of mutation on gating. In addition, R207C exhibits a much larger Cu^{2+}-dependent shift in the log(P_o)-V relation (Fig. 8 B) than the WT (Fig. 3 A), providing more direct evidence for an enhanced shift in voltage sensor activation for this mutant.

These results suggest that the relative position of side chains may change during voltage sensor activation, such that S1 and S4 coordinate Cu^{2+} better in the resting than the activated state, while S2 maintains a constant interaction with Cu^{2+}. A speculative model that illustrates this principal is depicted in Fig. 9 B, and is consistant with our data, but does not represent a unique solution.

The Cu^{2+} Binding Site Is Conserved in Shaker

Three of the four putative Cu^{2+}-coordinating residues in mSlo1 are charged (D133, D153, and R207) and highly conserved among voltage-gated K^+, Na^+, and Ca^{2+} channels (Fig. 6 A). This raises the possibility that many

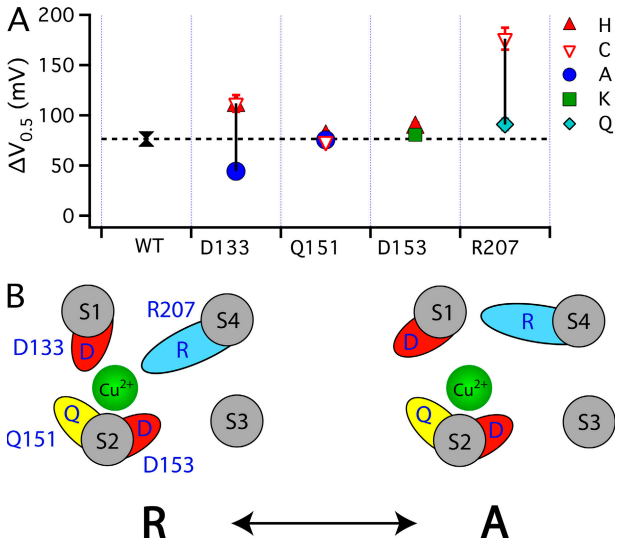

Figure 9. Effect of mutations on Cu^{2+}-efficacy. (A) The maximal G_K-V shift ($\Delta V_{0.5MAX}$) in response to saturating 1000 µM Cu^{2+} are plotted for the WT (⧗) and mutants at the four putative Cu^{2+}-coordinating sites (Ala: ●; Lys: ■; Gln: ◇; Cys: ▽; His: ▲). The dashed line indicates $\Delta V_{0.5MAX}$ for the WT. The vertical solid lines indicate the range of $\Delta V_{0.5MAX}$ for mutants at each position. (B) A speculative model of the Cu^{2+} binding site in the resting (R) and activated (A) state of the voltage sensor. In the resting state, Cu^{2+} is coordinated by D133(S1), Q151(S2), D153(S2), and R207(S4). The relative size and position of transmembrane segments correspond to those in the structure of a Kv1.2/Kv2.1 chimera (Long et al., 2007). During activation, the S2 residues interact with Cu^{2+} in a state-independent manner while interactions with D133 and R207 are weakened or disrupted, presumably by changes in the position or orientation of S1 and S4 relative to S2. In this way, mutation of any of these residues alter IC_{50}, but only mutation of D133 or R207 alter efficacy.

voltage-gated channels contain a metal binding site homologous to that in mSlo1. To test this possibility we examined the Cu^{2+} and Zn^{2+} sensitivity of Shaker K^+ channels (Fig. 10).

Previous studies have shown that 300 µM Zn^{2+} slows the activation kinetics of Shaker and shifts steady-state activation to more positive voltages (Boland et al., 1994). As in the case of mSlo1, we found that inactivation-removed Shaker (WT) was on the order of 100-fold more sensitive to extracellular Cu^{2+} than Zn^{2+} (Fig. 10, A–D). At −10 mV, the half-time to steady-state activation ($\tau_{0.5}$) of I_K was slowed approximately threefold and 15-fold in 5 µM and 20 µM Cu^{2+}, respectively, and 100 µM Cu^{2+} inhibited the current during a 50-ms pulse almost completely (Fig. 10 A). G_K-V relations (Fig. 10 B) were shifted progressively to more positive voltages by 5, 20, and 100 µM Cu^{2+} and exhibited a decrease in G_{Kmax} similar to mSlo1 (Fig. 2 A). Zn^{2+} had effects on Shaker activation kinetics (Fig. 10 C) and the G_K-V relation (Fig. 10 D) that were qualitatively similar to those of Cu^{2+} but occurred at much higher concentrations. Thus metal binding in Shaker, as in mSlo1, appears very selective for Cu^{2+} over Zn^{2+}.

Although Shaker can respond to low µM Cu^{2+} (e.g., 5 µM) it is evident from the small response to 1 µM Cu^{2+} (Fig. 10, A and B) that Shaker is less sensitive to Cu^{2+} than mSlo1. The G_K-V shift of Shaker by 100 µM Cu^{2+} (64 mV, Fig. 10 B) may be overestimated because the effect of Cu^{2+} on activation kinetics prevented achievement of steady-state activation during a 50-ms pulse at all but the most positive voltages tested. Given this caveat, the IC_{50} of Shaker approximated by fitting $V_{0.5}$-$[Cu^{2+}]$ from Fig. 10 B with $n_H = 1$ was 18 µM. This difference compared with the BK channel is consistent with the fact that mSlo1 contains a putative coordinating residue Q151 that is not conserved in Shaker, and that the Q151A mutation increases mSlo1's IC_{50} to 19.7 µM (Fig. 7 A).

To demonstrate that the metal binding site in Shaker is homologous to that in BK channels we examined the effects on Cu^{2+} and Zn^{2+} sensitivity of mutating S1 (E247) and S4 (R365) residues, corresponding to two of the three conserved coordinating sites in mSlo1 (Fig. 10, E–J). We tested for effects on activation kinetics since the kinetic changes complicated determination of steady-state activation. Mutation of E247 (D133 in mSlo1) to Ala (E247A) almost abolished the response to 5 µM Cu^{2+} and 1000 µM Zn^{2+} (Fig. 10, E and G), whereas E247C enhanced sensitivity to both Cu^{2+} (Fig. 10 F) and Zn^{2+} (Fig. 10 H). A similar result for Cu^{2+} was observed when R365 in S4 (R207 in mSlo1) was mutated to Ala (Fig. 10 I) or Cys (Fig. 10 J). In addition, similar to mSlo1, we observed that the response of WT Shaker to 5 µM Cu^{2+} was abolished at extracellular pH 5.2 (unpublished data). We did not investigate E283 in S2 (equivalent to D153 in mSlo1), because mutations at this position in Shaker expressed poorly in outside-out patches. Thus, we confirmed that two of the conserved Cu^{2+}-coordinating residues in mSlo1 also contribute to the Cu^{2+}/Zn^{2+} sensitivity of Shaker.

DISCUSSION

This study describes a previously unreported, rapid, and reversible inhibitory effect of extracellular Cu^{2+} on BK channel (mSlo1) activation at low micromolar and submicromolar concentrations. Cu^{2+} acts primarily to shift the voltage dependence of steady-state activation, together with lesser effects on G_{Kmax} and I_K kinetics. The G_K-V relation is shifted by up to 75 mV ($\Delta V_{0.5}$) with an IC_{50} of 2.0 µM Cu^{2+} and a Hill coefficient of 1.0 under our experimental conditions, and G_K can be reduced by >90% at voltages less than $V_{0.5}$. Thus BK channels are members of a small group of voltage-dependent channels that are extremely sensitive to physiologically relevant concentrations of Cu^{2+}; and mSlo1 may be the most Cu^{2+}-sensitive K^+ channel identified so far.

Biophysical and mutagenesis results indicate that Cu^{2+} binds in a state-dependent manner to the voltage sensor

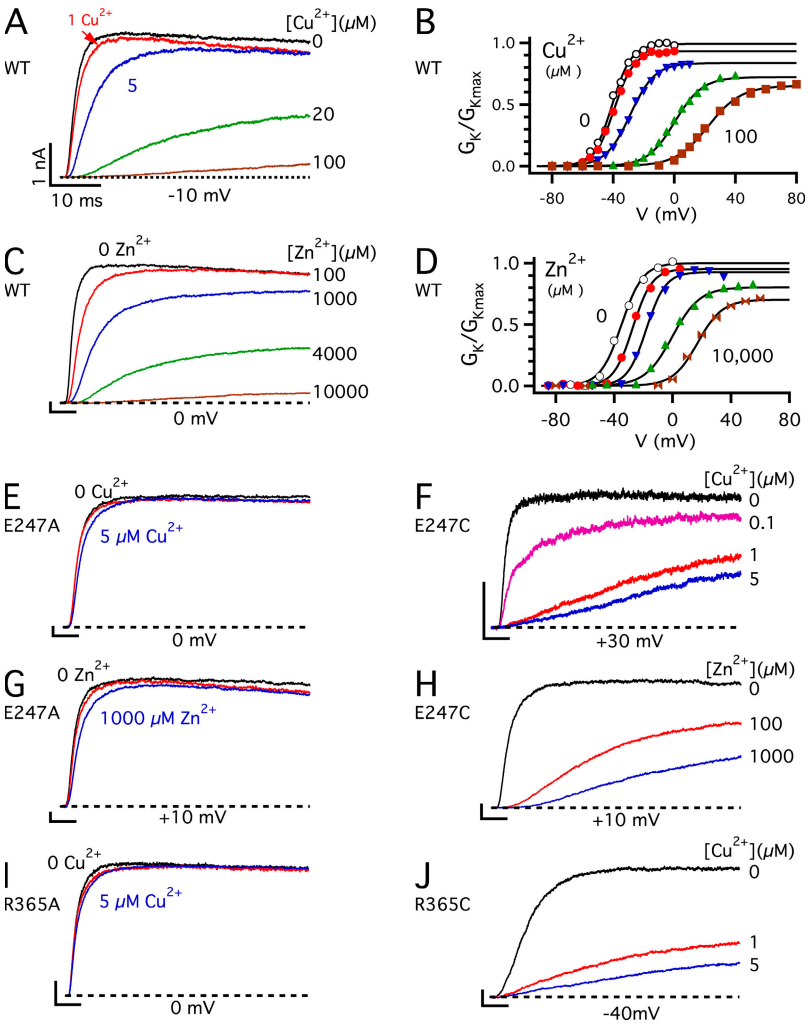

Figure 10. The Cu^{2+} coordination sites are conserved in Shaker channels. (A) I_K evoked from WT Shaker channels in response to pulses to −10 mV from a holding potential of −90 mV at the indicated $[Cu^{2+}]$ (0–100 μM). (B) G_K-V relations from the same patch in different $[Cu^{2+}]$ are normalized by G_{Kmax} in 0 Cu^{2+}. (0 (○), 1 (●), 5 (▼), 20 (▲), and 100 μM Cu^{2+} (■)). (C) I_K at 0 mV from WT channels at the indicated $[Zn^{2+}]$ (0–10,000 μM). (D) G_K-V relations in different $[Zn^{2+}]$, normalized by G_{Kmax} in 0 Zn^{2+} (0 (○), 100 (●), 1,000 (▼), 4,000 (▲), 10,000 μM Zn^{2+} (⧓)). (E) I_K at 0 mV from E247A channels in 0, 1, and 5 μM Cu^{2+}. (F) I_K at +30 mV from E247C in 0, 0.1, 1, and 5 μM Cu^{2+}. (G and H) I_K at +10 mV from E247A (G) or E247C (H) in 0, 100, and 1,000 μM Zn^{2+}. (I and J) I_K from R365A at 0 mV (I) or R365C at −40 mV(J) in 0, 1, and 5 μM Cu^{2+}. All Shaker experiments were performed from a holding potential of −90 mV. Most data were obtained in standard Shaker internal and external solutions (see Materials and methods) with the exception of R365 mutant data in I and J, which were obtained in a low chloride external solution with all but 10 mM Cl^- replaced by MeO_3^-, as in standard mSlo1 external solution.

domain where it interacts with transmembrane segments S1, S2, and S4, including acidic and basic residues that are highly conserved among most voltage-gated channels including Shaker. Native Cys and His residues do not contribute to the Cu^{2+} sensitivity of mSlo1. Likewise, native cysteines are not required for the Zn^{2+} sensitivity of Shaker (Boland et al., 1994). The binding site appears very selective for Cu^{2+} over closely related transition metals (Zn^{2+}, Cd^{2+}, Mn^{2+}, Fe^{3+}, Co^{2+}, and Ni^{2+}). Thus the voltage sensor can form a selective metal binding site with micromolar apparent affinity without requiring Cys or His residues that are often critical for the extreme metal sensitivity of other channels. We demonstrate here that Shaker K^+ channels can also respond to low micromolar Cu^{2+} and that some of the putative coordinating sites in mSlo1 are important for the Cu^{2+} and Zn^{2+} sensitivity of Shaker. Thus it is possible that our results define a metal binding site of general importance in voltage-gated channels.

Despite extensive investigation of metal coordination in enzymes, relatively little is known about metal binding sites in ion channels outside of the permeation pathway. In many cases, individual residues critical for the extreme sensitivity of particular channel subtypes have been identified, such as Cav3.2 and Nav1.5 (Satin et al., 1992; Jeong et al., 2003). In some cases, metal bridges that coordinate Cd^{2+} or Ni^{2+} between a pair of Cys and/or His residues have been defined in native channels (Gordon and Zagotta, 1995) or introduced by mutation (Holmgren et al., 1998; Webster et al., 2004). However, in few cases have potential coordinating residues been screened in sufficient detail to characterize a multivalent binding site. Importantly, we screened many residues in mSlo1, making multiple substitutions at most sites to inhibit and enhance Cu^{2+} sensitivity and to control for effects of mutations on gating. To confirm the direct participation of some positions in metal binding we also demonstrated effects of Cys or His substitution on Cd^{2+}/Cu^{2+} selectivity. In all, we identified four putative coordinating residues and 14 residues that do not contribute to Cu^{2+} sensitivity; both findings place constraints on the possible structure of the binding site. This detailed characterization together with the fact that putative coordinating sites are in transmembrane segments

of the voltage sensor and in most cases highly conserved among Kv channels allows us to use Kv channel structures as a framework for understanding what the binding site may look like and how it may change with gating. These and other implications of our results are discussed below.

Relation to Previous Studies

One reason that BK channels have not previously been recognized as extremely metal sensitive probably reflects their Cu^{2+} selectivity. Unlike Cav3.2, which is similarly sensitive to a number of transition metals, with IC_{50}s for Cu^{2+}, Zn^{2+}, and Ni^{2+} of 0.9, 2.1, and 4.9 µM (Kang et al., 2006), the BK channel responds poorly to metals other than Cu^{2+}. Another factor that may have masked the effect of Cu^{2+} is the state dependence of its action. Contrary to our results, a previous study failed to observe an acute response of single BK channels from rat skeletal muscle to 1–100 µM Cu^{2+} (Morera et al., 2003). This difference is unlikely to reflect that Morera et al. used a native channel reconstituted in lipid bilayers because they reported observing similar preliminary results with cloned hSlo1 channels expressed in *Xenopus* oocytes; the same preparation used here with a Slo1 homologue that is virtually identical to mSlo1. However, Morera et al. tested for the effect of Cu^{2+} under steady-state recording conditions where channels were maximally activated with $P_o \sim 0.9$ before Cu^{2+} was applied (V = +40 mV, $[Ca]_i$ = 60 µM). It is possible that these recording conditions prevented the acute effect of Cu^{2+} since mSlo1 channels that are maximally activated for 0.5 s are also insensitive to 100 µM Cu^{2+} (Fig. 3, C and D).

The IC_{50} for Cu^{2+} inhibition of mSlo1 G_K varied with voltage (0.53–2.24 µM, Fig. 2 D) but was in any case comparable to that reported previously for the most Cu^{2+}-sensitive Kv channel Kv1.3 (IC_{50} = 5.3 ± 0.5 µM) (Teisseyre and Mozrzymas, 2006) or the K2P "leak" channels Task-3 (IC_{50} = 2.7 ± 0.4 µM) and Trek-1 (EC_{50} = 3.0 ± 1.0 µM) (Gruss et al., 2004). However, the Cu^{2+} dose–response relation for mSlo1, characterized by a Hill coefficient ~1.0, is much shallower than that of Kv1.3 (n_H = 3.8), Trek-1 (n_H = 1.7 ± 0.8), or Task-3 (n_H = 1.8 ± 0.4). Therefore, with the caveat that these channels have not been studied under identical conditions, the BK channel is potentially the most Cu^{2+}-sensitive K^+ channel in that it has a lower threshold for response to Cu^{2+} (submicromolar), owing to its shallow dose–response relation.

We identified D153 as a coordinating site in mSlo1 because the corresponding residue in hERG is important for Cd^{2+} sensitivity (Fernandez et al., 2005). However, additional acidic coordinating sites in the S2 and S3 segments of hERG and dEAG are not conserved in mSlo1 (Fig. 6 A), suggesting the binding site in hERG and dEAG may be distinct from that in Slo1. Our results provide further support for this conclusion. First, we tested sites in S2 and S3 close to the positions that are important in hERG/dEAG and none were important for Cu^{2+} sensitivity in mSlo1. This included substituting Cys and Ala residues at a position in S2 (N158) that corresponds to a coordinating residue in hERG and dEAG. Conversely, the coordinating sites we identified in mSlo1 are largely absent from hERG or dEAG. The equivalent of D133 and Q151 in mSlo1 are aliphatic (I, V) in dEAG and hERG, and R207 is replaced by a lysine. Thus the binding sites of mSlo1 and dEAG may be distinct while mSlo1 and hERG share only a single acidic residue in S2.

Physiological Implications

The physiological importance of BK channel inhibition by Cu^{2+} is unknown. However, it is certainly intriguing that Slo1 appears poised to respond specifically to Cu^{2+} at concentrations estimated to be achieved in the synaptic cleft (Hopt et al., 2003). BK channel activation in nerve terminals is important for limiting action potential duration, Ca^{2+} entry, and neurotransmitter release (Faber and Sah, 2003). BK channels and Cu^{2+} are both present in glutamatergic synapses in the hippocampus (Kozma et al., 1981; Mathie et al., 2006; Misonou et al., 2006; Schlief and Gitlin, 2006). Thus the possibility exists that Cu^{2+} release could exert a positive feedback effect to enhance neurotransmitter and Cu^{2+} release by inhibiting BK channels in the same nerve terminal. Whether or not this could occur may depend on several factors including the metal sensitivity of Ca^{2+} channels in the nerve terminal as well as the time course of Cu^{2+} elevation. Because BK channels are less sensitive to Cu^{2+} when fully activated than at rest, it is possible they would respond less to release during an action potential than residual Cu^{2+} from preceding synaptic events. Another factor that could conceivably be important to the physiological response of BK channels is the effect of accessory β subunits. However, preliminary experiments indicated no appreciable effects on Cu^{2+} sensitivity of coexpressing mSlo1 with an excess of bovine β_1 (IC_{50} = 2.8 µM, n_H = 0.84, +220 mV, 0 Ca^{2+}) or human β_4 (IC_{50} = 2.7 µM, n_H = 0.95, +240 mV, 0 Ca^{2+}).

Shaker K^+ channels were found to be roughly 10-fold less sensitive to Cu^{2+} than mSlo1 in terms of IC_{50}. However the response of Shaker could also be physiologically relevant because, unlike mSlo1, Shaker activation kinetics were greatly slowed by Cu^{2+}. For example, 5 µM Cu^{2+} slowed activation kinetics threefold at −10 mV (Fig. 10 A) and might therefore greatly reduce the response to a brief action potential even though the effect of this concentration on steady-state activation was modest.

Mechanisms of Cu^{2+} Action

Several lines of evidence suggest that Cu^{2+} binds to the voltage sensor in a state-dependent manner to inhibit voltage sensor activation. First, Cu^{2+} shifts steady-state

activation (e.g., $V_{0.5}$) to more positive voltages, consistent with a shift in voltage sensor activation. Conversely, Cu^{2+} does not affect P_o at extreme negative voltages in the presence or absence of intracellular Ca^{2+} (Fig. 3 A), indicating that Cu^{2+} has little or no direct effect on channel opening or Ca^{2+}-dependent activation. Second, mutagenesis results define a site of action in the voltage sensor domain (Fig. 7). Third, mutation of some putative coordinating sites (D133 and R207) alter Cu^{2+} efficacy ($\Delta V_{0.5MAX}$), indicating that Cu^{2+} action does not depend merely on occupancy of its binding site, and consistent with a state-dependent interaction that favors Cu^{2+} binding to the resting state (Fig. 9). Fourth, the insensitivity of fully activated channels to Cu^{2+} (Fig. 3 B) also implies a state-dependent change in the affinity and/or access of the binding site. Finally, the dose–response relation for Cu^{2+} can be reproduced by a model that assumes Cu^{2+} binds in a state-dependent manner to the voltage sensor, as discussed below.

To a first approximation, the effect of Cu^{2+} on steady-state activation can be reproduced by a gating scheme illustrated in Fig. 11 A (Scheme 1), which assumes that Cu^{2+} binds with higher affinity to the resting than activated state of the voltage sensor. The best fit of this model to the $\Delta V_{0.5}$-$[Cu^{2+}]$ relation (Fig. 2 C, thick dotted curve) is almost identical to the Hill equation fit (solid curve) and yields Cu^{2+} dissociation constants for resting and activated states of 0.75 µM and 6.03 µM, respectively (see Fig. 2 legend for parameters).

Scheme 1 represents an extension of a well-established model that describes the effects of voltage and Ca^{2+} on BK channel activation (HA model) (Horrigan and Aldrich, 2002). The HA model (colored black in Scheme 1) asserts that a channel can undergo a closed to open (C-O) conformational change that is allosterically regulated by four independent and identical voltage sensors and Ca^{2+} sensors. Voltage sensors in each subunit equilibrate between resting (R) and activated (A), and Ca^{2+} sensors equilibrate between Ca^{2+} free (X) and Ca^{2+} bound (XCa^{2+}). Equilibrium constants for channel opening, voltage sensor activation, and Ca^{2+} binding are L, J, and K, respectively, where L and J are voltage dependent with partial charges z_L and z_J, and $K = [Ca^{2+}]/K_D$. The coupling between voltage sensor and gate is represented by an allosteric factor D such that the C-O equilibrium constant increases D-fold for each activated voltage sensor. Interactions of Ca^{2+} binding with the gate and voltage sensor are represented by allosteric factors C and E, respectively. Scheme 1 also assumes that each voltage sensor can equilibrate between Cu^{2+} free (Y) and Cu^{2+} bound (YCu^{2+}) with equilibrium constant $K_{Cu} = [Cu^{2+}]/K_{dCu}$ in the resting state and $E_{Cu}K_{Cu}$ in the activated state. E_{Cu} is an allosteric factor analogous to that describing the interaction between of Ca^{2+} and voltage sensors (E). The steady-state open probability predicted by Scheme 1 is defined by Eq. 1 (see next page).

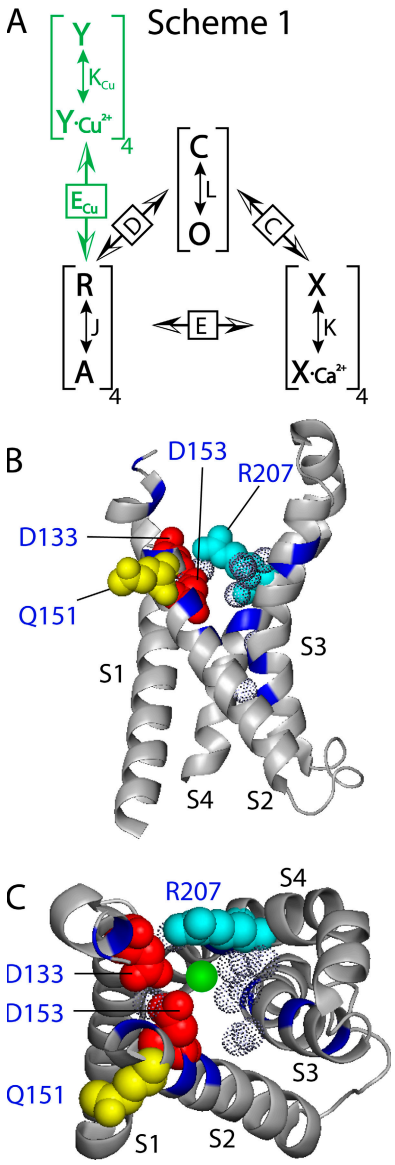

Figure 11. Mechanism and site of Cu^{2+} action. (A) Scheme 1 (see text), green indicates Cu^{2+}-dependent mechanisms, black represents HA model (Horrigan and Aldrich, 2002). (B and C) Residues mutated in mSlo1 are mapped onto the structure of a Kv1.2/Kv2.1 chimera (Long et al., 2007). B and C show side and top views, respectively. Only the S1–S4 segments from one subunit are shown with S1–S2 linker removed for clarity. Putative Cu^{2+}-coordinating residues were changed to the corresponding residue from mSlo1: D133(red), Q151(yellow), D153(red), R207(cyan). The backbone was colored dark blue at other positions that were tested. Dotted spheres indicate the position of water molecules in the structure. The green sphere illustrates a possible position for Cu^{2+}.

Scheme 1 requires only an 8.0-fold difference in affinity between resting and activated states ($E_{cu} = 0.124$) to account for the G_K-V shift by Cu^{2+}. Thus, the estimated K_ds of both the resting and activated states are much less than 100 µM, suggesting that the inability of 100 µM Cu^{2+} to inhibit fully activated channels in Fig. 3 C may reflect poor access to the binding site rather than a weak

$$P_o = \frac{L\left[(1+K_{Cu})(1+KC)+JD(1+K_{Cu}E_{Cu})(1+KCE)\right]^4}{L\left[(1+K_{Cu})(1+KC)+JD(1+K_{Cu}E_{Cu})(1+KCE)\right]^4+\left[(1+K_{Cu})(1+K)+J(1+K_{Cu}E_{Cu})(1+KE)\right]^4}, \quad (1)$$

$$\text{where } L = L_0 e^{\left(\frac{z_L V}{kT}\right)}; J = J_0 e^{\frac{z_J V}{kT}} = e^{\frac{z_J[V - V_{hC}]}{kT}}$$

interaction with the activated state. This conclusion is supported by the observation that mutation of sites in S2 (Q151 and D153) altered IC_{50} but not efficacy ($\Delta V_{0.5MAX}$, Fig. 9 A), suggesting these residues can interact with Cu^{2+} in the activated state.

Although Scheme 1 reproduces the $\Delta V_{0.5}$-$[Cu^{2+}]$ relation it does not account for all effects of Cu^{2+}. Scheme 1 predicts that the G_K-V in 3 µM Ca^{2+} should shift without decrease in slope (Fig. 2 F, curve A) or G_{Kmax}. However we observed that 100 µM Cu^{2+} reduced G_{Kmax} by 27% and reduced the slopes of the G_K-V and log(P_o)-V relations by 39% and 12%, respectively. Several mechanisms that could account for these effects are discussed below, but cannot currently be distinguished based on our data.

One mechanism that cannot account for effects of 100 µM Cu^{2+} on G_{Kmax} and G_K-V shape is the possibility raised by Fig. 3 C that Cu^{2+} cannot equilibrate with its binding site during a 30-ms depolarization. First, it is important to note that Cu^{2+} is equilibrated with the resting channel by the start of each voltage pulse, since the effect of 100 µM Cu^{2+} reaches a steady state within 1 s of application at −80 mV (Fig. 1 B) while the interval between pulses is 5 s. Second, 100 µM Cu^{2+} has a maximal effect on $V_{0.5}$ (Fig. 1 D and Fig. 2 C), implying that channels have a maximal number of Cu^{2+} bound when the G_K-V is measured, regardless of when or how fast Cu^{2+} reaches its binding site. Thus we conclude that decreases in G_{Kmax} and G-V slope in 100 µM Cu^{2+} reflect an equilibrium gating property of Cu^{2+}-bound channels.

Although Cu^{2+} equilibration kinetics cannot account for changes in G_K-V shape observed in saturating Cu^{2+}, they can affect the predictions of Scheme 1 and our estimate of K_{dCu}. To show this, we considered the extreme case that Cu^{2+} equilibrates at the holding potential but cannot bind or dissociate during a voltage pulse. Thus, the probability that a voltage sensor is Cu^{2+} bound ($P_{Cu}[Cu^{2+}]$) is determined only by the K_d of the resting state (K_{dCu}), and the distribution of channel species with different numbers of Cu^{2+} bound (i = 0–4) is determined by a binomial distribution where each species has a different open probability ($P_O[i]$) specified by Scheme 1. Mean open probability in this case is given by Eq. 2 (see below).

Eq. 2 can fit the $\Delta V_{0.5}$-$[Cu^{2+}]$ relation (Fig. 2 C, thin dotted curve) with a value of E_{Cu} = 0.129 similar to that determined from Eq. 1 (0.124). However, the value of K_{dCu} from Eq. 2 (2.1 µM) is comparable to the IC_{50} and therefore greater than predicted by Eq. 1 (0.75 µM). An interesting property of Eq. 2 is it predicts a decrease in G_K-V slope (z_{APP}) at intermediate $[Cu^{2+}]$ (Fig. 2 F, curve B). However, this slope decrease is a consequence of heterogeneity in the number of Cu^{2+} bound to each channel rather than a property of any one species ($P_o[i]$), and therefore does not persist in saturating Cu^{2+}.

The decreased slope of the log(P_o)-V relation observed in saturating Cu^{2+}, according to the HA model, can only be caused by a decrease in gating charge or a decrease in voltage sensor/gate coupling (D-factor) (Ma et al., 2006). Either of these mechanisms is possible. One of the putative coordinating sites for Cu^{2+}, D153, is thought to be a voltage-sensing residue in Slo1 in part because a charge reversal at this position (D153K) reduces the slope of log(P_o)-V by almost 50% (Ma et al., 2006). If Cu^{2+} remains associated with D153 during voltage sensor activation it might in effect reverse the net charge of this residue and reduce gating charge. It would also be possible for Cu^{2+} to reduce voltage sensor/gate coupling if its binding depends on the open state of the channel as well as the activation state of the voltage sensor. Intracellular ligands in Slo1 are known to have such effects on voltage sensor/gate coupling (Horrigan et al., 2005; Horrigan and Ma, 2008).

The decrease in G_{Kmax} by Cu^{2+} was observed at all $[Ca^{2+}]$ tested (0–10 µM) and is not caused by a decrease in single channel conductance (Fig. 1 C) or a failure to measure steady-state activation since Cu^{2+} had a relatively minor effect on I_K kinetics in mSlo1 (Fig. 1 F). These results cannot be accounted for by Scheme 1 or the HA model because any mechanism that decreases the C-O equilibrium constant (L) to reduce G_{Kmax} in 0 Ca^{2+} should be overcome by the ability of Ca^{2+} to increase L more than 100-fold at 5–10 µM concentrations

$$P_o = \sum_{i=0}^{4} P_o[i] \frac{4!}{i!(4-i)!} P_{Cu}{}^{i} (1-P_{Cu})^{(4-i)}, \text{ where } P_{Cu} = \frac{[Cu^{2+}]}{[Cu^{2+}]+K_{dCu}} \text{ and}$$

$$P_o[i] = \frac{L\left[(1+KC)+JD(1+KCE)\right]^{(4-i)}\left[(1+KC)+JDE_{Cu}(1+KCE)\right]^{i}}{L\left[(1+KC)+JD(1+KCE)\right]^{(4-i)}\left[(1+KC)+JDE_{Cu}(1+KCE)\right]^{i}+\left[(1+K)+J(1+KE)\right]^{(4-i)}\left[(1+K)+JE_{Cu}(1+KE)\right]^{i}} \quad (2)$$

(Horrigan and Aldrich, 2002). That Cu^{2+} reduced G_{Kmax} by a similar amount in different $[Ca^{2+}]_i$ suggests that a fraction of channels enter a nonconducting state that is not included in our model. Metal binding to the pore domain of Kv1.5 has been proposed to reduce G_{Kmax} by stabilizing a slow inactivated state (Kehl et al., 2002). Such a mechanism seems unlikely since Slo1 is not known to inactivate in the absence of β subunits. However, BK channels have been reported to enter brief "flicker" closed states that are not included in the HA model and limit the maximum open probability of BK channels to ~0.9 in all $[Ca^{2+}]_i$(Rothberg and Magleby, 1998). Therefore it is conceivable such states could be stabilized by Cu^{2+} to reduce G_{Kmax} in a Ca^{2+}-independent manner.

Structure and Function of the Cu^{2+} Binding Site

The detailed structure of the BK channel is unknown. However, the putative Cu^{2+}-coordinating residues in mSlo1 are for the most part conserved in other voltage-gated channels, including Kv channels of known structure (Fig. 6 A). We have also confirmed that S1 and S4 residues, corresponding to D133 and R207 in mSlo1, are important for the Cu^{2+} and Zn^{2+} sensitivity of Shaker (Fig. 10). Thus it is likely we can gain insight into the properties of this site by examining the structure of Kv channels.

The crystal structures of several Kv channels have been solved in the activated conformation (Jiang et al., 2003; Long et al., 2005a; Long et al., 2007). In Fig. 11 (B and C) we mapped the putative Cu^{2+}-coordinating residues from mSlo1 onto the highest resolution example, a Kv1.2/Kv2.2 chimera (Long et al., 2007), based on the sequence alignment in Fig. 6 A. Although our results suggest this structure in the activated conformation should not be ideal for Cu^{2+} binding, it does provide some important insight. First, a cavity is present between the S1–S4 transmembrane segments that contains water molecules (dotted spheres) and therefore can presumably accommodate metal ions. Second, the three most highly conserved putative Cu^{2+}-coordinating residues in S1(D133), S2(D153), and S4(R207) face each other in the crystal structure to form what looks like a reasonable binding pocket (Fig. 11 C). Although the fourth putative Cu^{2+}-coordinating residue (Q151) faces away from the others in the crystal structure (toward lipid), it is conceivable that S2 in mSlo1 might adopt a different orientation to allow both Q151 and D153 to participate in Cu^{2+} binding (as illustrated in Fig. 9 B). Third, all four putative coordinating residues are distributed around the cavity, near the top of the voltage sensor, and roughly define a plane when viewed from the side (Fig. 11 B). This distribution may help explain the Cu^{2+} selectivity of the BK channel since the most favored coordination geometry for Cu^{2+} is square planar (Rulisek and Vondrasek, 1998). That many sites above and below the putative coordinating residues did not contribute to Cu^{2+} sensitivity in mSlo1 (backbone colored dark blue) is also consistent with a planar coordination geometry. However it should be noted that other than Cys, His, and acidic residues, extracellular loops were not tested in detail and could potentially participate in metal binding through backbone interactions. Finally, the acidic coordinating residues D133 and D153 are present on antiparallel helices (S1 and S2) and contact each other (in Kv1.2), consistent with the possibility that their pKa's are perturbed to account for the pH sensitivity of Cu^{2+} action (Fig. 5 D). Such an interaction would tend to increase the pKa of one partner and decrease the other. Additional factors that could increase pKa include the presence of D133 at the C terminus of a helix and the location of these residues near an aqueous crevice (Forsyth et al., 2002).

Our results suggest that Cu^{2+} should bind better in the resting than the activated conformation. Therefore it is reasonable to expect that the relative position of the four putative coordinating residues may change during activation. Recent studies based on a variety of approaches suggest that S4 may undergo a large motion relative to S1 and S2 during activation in Kv channels (Campos et al., 2007; Long et al., 2007; Pathak et al., 2007). Such a motion is qualitatively consistent with the formation of a state-dependent binding site between S1, S2, and S4. However, it should be noted that this gating motion is likely larger in Kv channels than in BK channels, which are weakly voltage dependent. Indeed we have suggested previously that the resting conformation of mSlo1 may be similar to an intermediate activated state of Shaker (Ma et al., 2006). It is possible that Cu^{2+} slowed the activation of Shaker (Fig. 10 A) more than mSlo1 (Fig. 1 E) by stabilizing an intermediate state in Shaker. However another reason for this difference is that voltage sensor activation is rate limiting for I_K activation in Shaker, whereas the closed–open transition is rate limiting in Slo1 (Horrigan and Aldrich, 2002). Thus a slowing of voltage sensor activation by Cu^{2+} could increase the time constant of I_K activation in Shaker while altering primarily the delay in activation of Slo1 (Horrigan and Aldrich, 1999).

This work was supported by a grant from the National Institutes of Health (NS42901) to F.T. Horrigan. An abstract of this work was presented at the 50th Annual Meeting of the Biophysical society (2006).

Olaf S. Andersen served as editor.

Submitted: 4 February 2008
Accepted: 1 April 2008

REFERENCES

Armstrong, C.M., and F. Bezanilla. 1974. Charge movement associated with the opening and closing of the activation gates of the Na channels. *J. Gen. Physiol.* 63:533–552.

Assaf, S.Y., and S.H. Chung. 1984. Release of endogenous Zn^{2+} from brain tissue during activity. *Nature.* 308:734–736.

Berkovitch, F., Y. Nicolet, J.T. Wan, J.T. Jarrett, and C.L. Drennan. 2004. Crystal structure of biotin synthase, an S-adenosylmethionine-dependent radical enzyme. *Science.* 303:76–79.

Bewley, M.C., P.D. Jeffrey, M.L. Patchett, Z.F. Kanyo, and E.N. Baker. 1999. Crystal structures of *Bacillus caldovelox* arginase in complex with substrate and inhibitors reveal new insights into activation, inhibition and catalysis in the arginase superfamily. *Structure.* 7:435–448.

Boland, L.M., M.E. Jurman, and G. Yellen. 1994. Cysteines in the Shaker K^+ channel are not essential for channel activity or zinc modulation. *Biophys. J.* 66:694–699.

Bush, A.I. 2000. Metals and neuroscience. *Curr. Opin. Chem. Biol.* 4:184–191.

Butler, A., S. Tsunoda, D.P. McCobb, A. Wei, and L. Salkoff. 1993. mSlo, a complex mouse gene encoding "maxi" calcium-activated potassium channels. *Science.* 261:221–224.

Campos, F.V., B. Chanda, B. Roux, and F. Bezanilla. 2007. Two atomic constraints unambiguously position the S4 segment relative to S1 and S2 segments in the closed state of Shaker K channel. *Proc. Natl. Acad. Sci. USA.* 104:7904–7909.

Castelli, L., F. Tanzi, V. Taglietti, and J. Magistretti. 2003. Cu^{2+}, Co^{2+}, and Mn^{2+} modify the gating kinetics of high-voltage-activated Ca^{2+} channels in rat palaeocortical neurons. *J. Membr. Biol.* 195:121–136.

Colquhoun, D. 1998. Binding, gating, affinity and efficacy: the interpretation of structure-activity relationships for agonists and of the effects of mutating receptors. *Br. J. Pharmacol.* 125:924–947.

Cox, D.H., J. Cui, and R.W. Aldrich. 1997. Allosteric gating of a large conductance Ca^{2+}-activated K^+ channel. *J. Gen. Physiol.* 110:257–281.

Cui, J., and R.W. Aldrich. 2000. Allosteric linkage between voltage and Ca^{2+}-dependent activation of BK-type mslo1 K^+ channels. *Biochemistry.* 39:15612–15619.

Di Costanzo, L., L.V. Flores Jr., and D.W. Christianson. 2006. Stereochemistry of guanidine-metal interactions: implications for L-arginine-metal interactions in protein structure and function. *Proteins.* 65:637–642.

Diaz, F., M. Wallner, E. Stefani, L. Toro, and R. Latorre. 1996. Interaction of internal Ba^{2+} with a cloned Ca^{2+}-dependent K^+ (hslo) channel from smooth muscle. *J. Gen. Physiol.* 107:399–407.

Elinder, F., and P. Arhem. 2003. Metal ion effects on ion channel gating. *Q. Rev. Biophys.* 36:373–427.

Faber, E.S., and P. Sah. 2003. Calcium-activated potassium channels: multiple contributions to neuronal function. *Neuroscientist.* 9:181–194.

Ferguson, W.B. 1991. Competitive Mg^{2+} block of a large-conductance, Ca^{2+}-activated K^+ channel in rat skeletal muscle. Ca^{2+}, Sr^{2+}, and Ni^{2+} also block. *J. Gen. Physiol.* 98:163–181.

Fernandez, D., A. Ghanta, K.I. Kinard, and M.C. Sanguinetti. 2005. Molecular mapping of a site for Cd^{2+}-induced modification of human ether-a-go-go-related gene (hERG) channel activation. *J. Physiol.* 567:737–755.

Ferraroni, M., S. Tilli, F. Briganti, W.R. Chegwidden, C.T. Supuran, K.E. Wiebauer, R.E. Tashian, and A. Scozzafava. 2002. Crystal structure of a zinc-activated variant of human carbonic anhydrase I, CA I Michigan 1: evidence for a second zinc binding site involving arginine coordination. *Biochemistry.* 41:6237–6244.

Forsyth, W.R., J.M. Antosiewicz, and A.D. Robertson. 2002. Empirical relationships between protein structure and carboxyl pKa values in proteins. *Proteins.* 48:388–403.

Frederickson, C.J., L.J. Giblin III, R.V. Balaji, R. Masalha, Y. Zeng, E.V. Lopez, J.Y. Koh, U. Chorin, L. Besser, M. Hershfinkel, et al. 2006. Synaptic release of zinc from brain slices: factors governing release, imaging, and accurate calculation of concentration. *J. Neurosci. Methods.* 154:19–29.

Frederickson, C.J., J.Y. Koh, and A.I. Bush. 2005. The neurobiology of zinc in health and disease. *Nat. Rev. Neurosci.* 6:449–462.

Gilly, W.F., and C.M. Armstrong. 1982a. Divalent cations and the activation kinetics of potassium channels in squid giant axons. *J. Gen. Physiol.* 79:965–996.

Gilly, W.F., and C.M. Armstrong. 1982b. Slowing of sodium channel opening kinetics in squid axon by extracellular zinc. *J. Gen. Physiol.* 79:935–964.

Gordon, S.E., and W.N. Zagotta. 1995. Subunit interactions in coordination of Ni^{2+} in cyclic nucleotide-gated channels. *Proc. Natl. Acad. Sci. USA.* 92:10222–10226.

Gruss, M., A. Mathie, W.R. Lieb, and N.P. Franks. 2004. The two-pore-domain K^+ channels TREK-1 and TASK-3 are differentially modulated by copper and zinc. *Mol. Pharmacol.* 66:530–537.

Hamill, O.P., A. Marty, E. Neher, B. Sakmann, and F.J. Sigworth. 1981. Improved patch-clamp techniques for high-resolution current recording from cells and cell-free membrane patches. *Pflugers Arch.* 391:85–100.

Hartter, D.E., and A. Barnea. 1988. Evidence for release of copper in the brain: depolarization-induced release of newly taken-up 67copper. *Synapse.* 2:412–415.

Herrington, J., and R.J. Bookman. 1995. Pulse Control. University of Miami Press, Miami, FL.

Hidmi, L., and M. Edwards. 1999. Role of temperature and pH in $Cu(OH)_2$ solubility. *Environ. Sci. Technol.* 33:2607–2610.

Holmgren, M., K.S. Shin, and G. Yellen. 1998. The activation gate of a voltage-gated K^+ channel can be trapped in the open state by an intersubunit metal bridge. *Neuron.* 21:617–621.

Hopt, A., S. Korte, H. Fink, U. Panne, R. Niessner, R. Jahn, H. Kretzschmar, and J. Herms. 2003. Methods for studying synaptosomal copper release. *J. Neurosci. Methods.* 128:159–172.

Horrigan, F.T., and R.W. Aldrich. 1999. Allosteric voltage gating of potassium channels II. Mslo channel gating charge movement in the absence of Ca^{2+}. *J. Gen. Physiol.* 114:305–336.

Horrigan, F.T., and R.W. Aldrich. 2002. Coupling between voltage sensor activation, Ca^{2+} binding and channel opening in large conductance (BK) potassium channels. *J. Gen. Physiol.* 120:267–305.

Horrigan, F.T., J. Cui, and R.W. Aldrich. 1999. Allosteric voltage gating of potassium channels I. Mslo ionic currents in the absence of Ca^{2+}. *J. Gen. Physiol.* 114:277–304.

Horrigan, F.T., S.H. Heinemann, and T. Hoshi. 2005. Heme regulates allosteric activation of the Slo1 BK channel. *J. Gen. Physiol.* 126:7–21.

Horrigan, F.T., and Z. Ma. 2008. Mg^{2+} enhances voltage sensor/gate coupling in BK channels. *J. Gen. Physiol.* 131:13–32.

Howell, G.A., M.G. Welch, and C.J. Frederickson. 1984. Stimulation-induced uptake and release of zinc in hippocampal slices. *Nature.* 308:736–738.

Hu, L., H. Yang, J. Shi, and J. Cui. 2006. Effects of multiple metal binding sites on calcium and magnesium-dependent activation of BK channels. *J. Gen. Physiol.* 127:35–49.

Huidobro-Toro, J.P., R.A. Lorca, and C. Coddou. 2008. Trace metals in the brain: allosteric modulators of ligand-gated receptor channels, the case of ATP-gated P2X receptors. *Eur. Biophys J.* 37:301–314.

Jeong, S.W., B.G. Park, J.Y. Park, J.W. Lee, and J.H. Lee. 2003. Divalent metals differentially block cloned T-type calcium channels. *Neuroreport.* 14:1537–1540.

Jiang, Y., A. Lee, J. Chen, V. Ruta, M. Cadene, B.T. Chait, and R. MacKinnon. 2003. X-ray structure of a voltage-dependent K^+ channel. *Nature.* 423:33–41.

Kang, H.W., J.Y. Park, S.W. Jeong, J.A. Kim, H.J. Moon, E. Perez-Reyes, and J.H. Lee. 2006. A molecular determinant of nickel inhibition in Cav3.2 T-type calcium channels. *J. Biol. Chem.* 281:4823–4830.

Kardos, J., I. Kovacs, F. Hajos, M. Kalman, and M. Simonyi. 1989. Nerve endings from rat brain tissue release copper upon depolarization. A possible role in regulating neuronal excitability. *Neurosci. Lett.* 103:139–144.

Kehl, S.J., C. Eduljee, D.C. Kwan, S. Zhang, and D. Fedida. 2002. Molecular determinants of the inhibition of human Kv1.5 potassium currents by external protons and Zn^{2+}. *J. Physiol.* 541:9–24.

Kiss, T., and O.N. Osipenko. 1994. Toxic effects of heavy metals on ionic channels. *Pharmacol. Rev.* 46:245–267.

Kozma, M., P. Szerdahelyi, and P. Kasa. 1981. Histochemical detection of zinc and copper in various neurons of the central nervous system. *Acta Histochem.* 69:12–17.

Li, Y., C.J. Hough, S.W. Suh, J.M. Sarvey, and C.J. Frederickson. 2001. Rapid translocation of Zn^{2+} from presynaptic terminals into postsynaptic hippocampal neurons after physiological stimulation. *J. Neurophysiol.* 86:2597–2604.

Linder, M.C., and M. Hazegh-Azam. 1996. Copper biochemistry and molecular biology. *Am. J. Clin. Nutr.* 63:797S–811S.

Liu, J., M. Zhang, M. Jiang, and G.N. Tseng. 2003. Negative charges in the transmembrane domains of the HERG K^+ channel are involved in the activation- and deactivation-gating processes. *J. Gen. Physiol.* 121:599–614.

Long, S.B., E.B. Campbell, and R. Mackinnon. 2005a. Crystal structure of a mammalian voltage-dependent Shaker family K^+ channel. *Science.* 309:897–903.

Long, S.B., E.B. Campbell, and R. Mackinnon. 2005b. Voltage sensor of Kv1.2: structural basis of electromechanical coupling. *Science.* 309:903–908.

Long, S.B., X. Tao, E.B. Campbell, and R. MacKinnon. 2007. Atomic structure of a voltage-dependent K^+ channel in a lipid membrane-like environment. *Nature.* 450:376–382.

Ma, Z., X.J. Lou, and F.T. Horrigan. 2006. Role of charged residues in the S1-S4 voltage sensor of BK channels. *J. Gen. Physiol.* 127:309–328.

MacKinnon, R., R. Latorre, and C. Miller. 1989. Role of surface electrostatics in the operation of a high-conductance Ca^{2+}-activated K^+ channel. *Biochemistry.* 28:8092–8099.

Mash, H.E., Y.P. Chin, L. Sigg, R. Hari, and H. Xue. 2003. Complexation of copper by zwitterionic aminosulfonic (good) buffers. *Anal. Chem.* 75:671–677.

Mathie, A., G.L. Sutton, C.E. Clarke, and E.L. Veale. 2006. Zinc and copper: pharmacological probes and endogenous modulators of neuronal excitability. *Pharmacol. Ther.* 111:567–583.

Misonou, H., M. Menegola, L. Buchwalder, E.W. Park, A. Meredith, K.J. Rhodes, R.W. Aldrich, and J.S. Trimmer. 2006. Immunolocalization of the Ca^{2+}-activated K^+ channel Slo1 in axons and nerve terminals of mammalian brain and cultured neurons. *J. Comp. Neurol.* 496:289–302.

Morera, F.J., D. Wolff, and C. Vergara. 2003. External copper inhibits the activity of the large-conductance calcium- and voltage-sensitive potassium channel from skeletal muscle. *J. Membr. Biol.* 192:65–72.

Nelson, M.T., P.M. Joksovic, P. Su, H.W. Kang, A. Van Deusen, J.P. Baumgart, L.S. David, T.P. Snutch, P.Q. Barrett, J.H. Lee, et al. 2007. Molecular mechanisms of subtype-specific inhibition of neuronal T-type calcium channels by ascorbate. *J. Neurosci.* 27:12577–12583.

Neyton, J. 1996. A Ba^{2+} chelator suppresses long shut events in fully activated high-conductance Ca^{2+}-dependent K^+ channels. *Biophys. J.* 71:220–226.

Oberhauser, A., O. Alvarez, and R. Latorre. 1988. Activation by divalent cations of a Ca^{2+}-activated K^{2+} channel from skeletal muscle membrane. *J. Gen. Physiol.* 92:67–86.

Ono, S., and M.G. Cherian. 1999. Regional distribution of metallothionein, zinc, and copper in the brain of different strains of rats. *Biol. Trace Elem. Res.* 69:151–159.

Osterberg, R. 1980. Physiology and pharmacology of copper. *Pharmacol. Ther.* 9:121–146.

Pathak, M.M., V. Yarov-Yarovoy, G. Agarwal, B. Roux, P. Barth, S. Kohout, F. Tombola, and E.Y. Isacoff. 2007. Closing in on the resting state of the shaker K^+ channel. *Neuron.* 56:124–140.

Pivovarov, S. 2005. Modeling of ionic equilibria of trace metals (Cu^{2+}, Zn^{2+}, Cd^{2+}) in concentrated aqueous electrolyte solutions at 25°C. *J. Colloid Interface Sci.* 291:421–432.

Rothberg, B.S., and K.L. Magleby. 1998. Kinetic structure of large-conductance Ca^{2+}-activated K^+ channels suggests that the gating includes transitions through intermediate or secondary states. A mechanism for flickers. *J. Gen. Physiol.* 111:751–780.

Rulisek, L., and J. Vondrasek. 1998. Coordination geometries of selected transition metal ions (Co^{2+}, Ni^{2+}, Cu^{2+}, Zn^{2+}, Cd^{2+}, and Hg^{2+}) in metalloproteins. *J. Inorg. Biochem.* 71:115–127.

Satin, J., J.W. Kyle, M. Chen, P. Bell, L.L. Cribbs, H.A. Fozzard, and R.B. Rogart. 1992. A mutant of TTX-resistant cardiac sodium channels with TTX-sensitive properties. *Science.* 256:1202–1205.

Sato, M., K. Ohtomo, T. Daimon, T. Sugiyama, and K. Iijima. 1994. Localization of copper to afferent terminals in rat locus ceruleus, in contrast to mitochondrial copper in cerebellum. *J. Histochem. Cytochem.* 42:1585–1591.

Schlief, M.L., and J.D. Gitlin. 2006. Copper homeostasis in the CNS: a novel link between the NMDA receptor and copper homeostasis in the hippocampus. *Mol. Neurobiol.* 33:81–90.

Silverman, W.R., C.Y. Tang, A.F. Mock, K.B. Huh, and D.M. Papazian. 2000. Mg^{2+} modulates voltage-dependent activation in ether-a-go-go potassium channels by binding between transmembrane segments S2 and S3. *J. Gen. Physiol.* 116:663–678.

Silverman, W.R., J.P. Bannister, and D.M. Papazian. 2004. Binding site in eag voltage sensor accommodates a variety of ions and is accessible in closed channel. *Biophys. J.* 87:3110–3121.

Slomianka, L., G. Danscher, and C.J. Frederickson. 1990. Labeling of the neurons of origin of zinc-containing pathways by intraperitoneal injections of sodium selenite. *Neuroscience.* 38:843–854.

Sokolowska, M., and W. Bal. 2005. Cu(II) complexation by "non-coordinating" N-2-hydroxyethylpiperazine-N'-2-ethanesulfonic acid (HEPES buffer). *J. Inorg. Biochem.* 99:1653–1660.

Takeda, A. 2000. Movement of zinc and its functional significance in the brain. *Brain Res. Brain Res. Rev.* 34:137–148.

Teisseyre, A., and J.W. Mozrzymas. 2006. The inhibitory effect of copper ions on lymphocyte Kv1.3 potassium channels. *J. Physiol. Pharmacol.* 57:301–314.

Thompson, R.B., D. Peterson, W. Mahoney, M. Cramer, B.P. Maliwal, S.W. Suh, C. Frederickson, C. Fierke, and P. Herman. 2002. Fluorescent zinc indicators for neurobiology. *J. Neurosci. Methods.* 118:63–75.

Webster, S.M., D. Del Camino, J.P. Dekker, and G. Yellen. 2004. Intracellular gate opening in Shaker K^+ channels defined by high-affinity metal bridges. *Nature.* 428:864–868.

Yang, H., L. Hu, J. Shi, K. Delaloye, F.T. Horrigan, and J. Cui. 2007. Mg^{2+} mediates interaction between the voltage sensor and cytosolic domain to activate BK channels. *Proc. Natl. Acad. Sci. USA.* 104:18270–18275.

Yellen, G., D. Sodickson, T.Y. Chen, and M.E. Jurman. 1994. An engineered cysteine in the external mouth of a K^+ channel allows inactivation to be modulated by metal binding. *Biophys. J.* 66:1068–1075.2.